JOURNAL OF GEOPHYSICAL RESEARCH, VOL. 113, B06101, doi:10.1029/2007JB005499, 2008

Pacific absolute plate motion since 145 Ma: An assessment of the fixed hot spot hypothesis

Paul Wessel[1] and Loren W. Kroenke[1]

Received 13 November 2007; revised 12 February 2008; accepted 28 February 2008; published 5 June 2008.

[1] Using the geometry and ages from 12 Pacific seamount chains, we have determined two new absolute plate motion models that now extend our self-consistent and high-resolution models with covariance estimates back to 145 Ma. The WK08-A model maps the full uncertainty in the age progressions into uncertainties in rotation opening angles, yielding a relatively smooth plate motion model. The WK08-G model relaxes the mapping of age uncertainties in order to better isolate secondary geometry changes seen along many coregistered chains. Both models have been used to assess the viability of the fixed hot spot hypothesis in the Pacific. In determining the models, we found that only a small group of age samples had to be discarded on the grounds that they were discordant with the dominant trends. We were able to connect plate motions for pre- and post-Emperor age intervals by including the Ratak-Gilbert-Ellice and Musicians trails in our analysis. However, as no active hot spot locations exist for the older chains, their inclusion adds additional model parameters. Both age and geometry misfits increase with age, reflecting the observed increase in age uncertainties and the general widening of trails. Secondary (and short-lived) changes in absolute plate motion mapped in WK08-G appear to correlate with the timing and sense of motion of known Pacific Rim tectonic events. Analysis of interchain distances between coeval samples from the Hawaii and Louisville chains suggests possible discrepancies during the older Emperor stage that are compatible with predictions of hot spot drift. We computed a new apparent polar wander path for the Pacific and found a high degree of correspondence with paleomagnetically derived paths, as long as solutions allowing for anomalous skewness were included in the latter. Our polar wander path suggests that there might have been some true polar wander during the Emperor stage, complemented by a smaller amount of hot spot drift than otherwise required. We show that chain geometries and ages, combined with future paleolatitude determinations from additional sites and chains could enable an observation-based description of both hot spot and plate motions without relying on predictions of hot spot drift derived from mantle flow calculations.

Citation: Wessel, P., and L. W. Kroenke (2008), Pacific absolute plate motion since 145 Ma: An assessment of the fixed hot spot hypothesis, *J. Geophys. Res.*, *113*, B06101, doi:10.1029/2007JB005499.

1. Introduction

[2] The observations that (1) volcano ages monotonically increase away from the most recent site of activity along a chain [e.g., *Dana*, 1849] and (2) several seamount and island chains appear to have colinear geometries gave rise to the fixed hot spot hypothesis [*Morgan*, 1971; *Wilson*, 1963]. In this hypothesis, hot spots are the surface manifestations of deep mantle plumes that are stable over long time intervals and may therefore define a fixed reference system (i.e., the hot spot reference frame). As the Earth's tectonic plates move over the mantle, volcanoes are produced over the fixed hot spots and their geometric alignments and age progressions may therefore be used to decipher the history of what we call absolute plate motions (APM).

[3] One straightforward interpretation of the surface evidence is *Wilson's* [1963] classic suggestion that the $\sim$120° bend in the Hawaii-Emperor chain simply reflects a $\sim$60° change in Pacific APM. Lately, this explanation has been questioned since the volcanoes making up the Emperor Seamount chain apparently formed at significantly more northerly latitudes than the present latitude of the Hawaii hot spot would imply [e.g., *Tarduno and Cottrell*, 1997; *Tarduno et al.*, 2003]. Careful assessment of paleomagnetic poles derived from drill cores elsewhere, seamount magnetizations, and marine magnetic anomaly skewness data corroborate these findings [e.g., *Beaman et al.*, 2007]. Thus, as the other end-member possibility, the paleomagnetic data have been interpreted to imply that the formation of the Hawaii-Emperor bend (HEB) simply was accommodated by

[1]School of Ocean and Earth Science and Technology, University of Hawaii at Manoa, Honolulu, Hawaii, USA.

0148-0227/08/2007JB005499$09.00

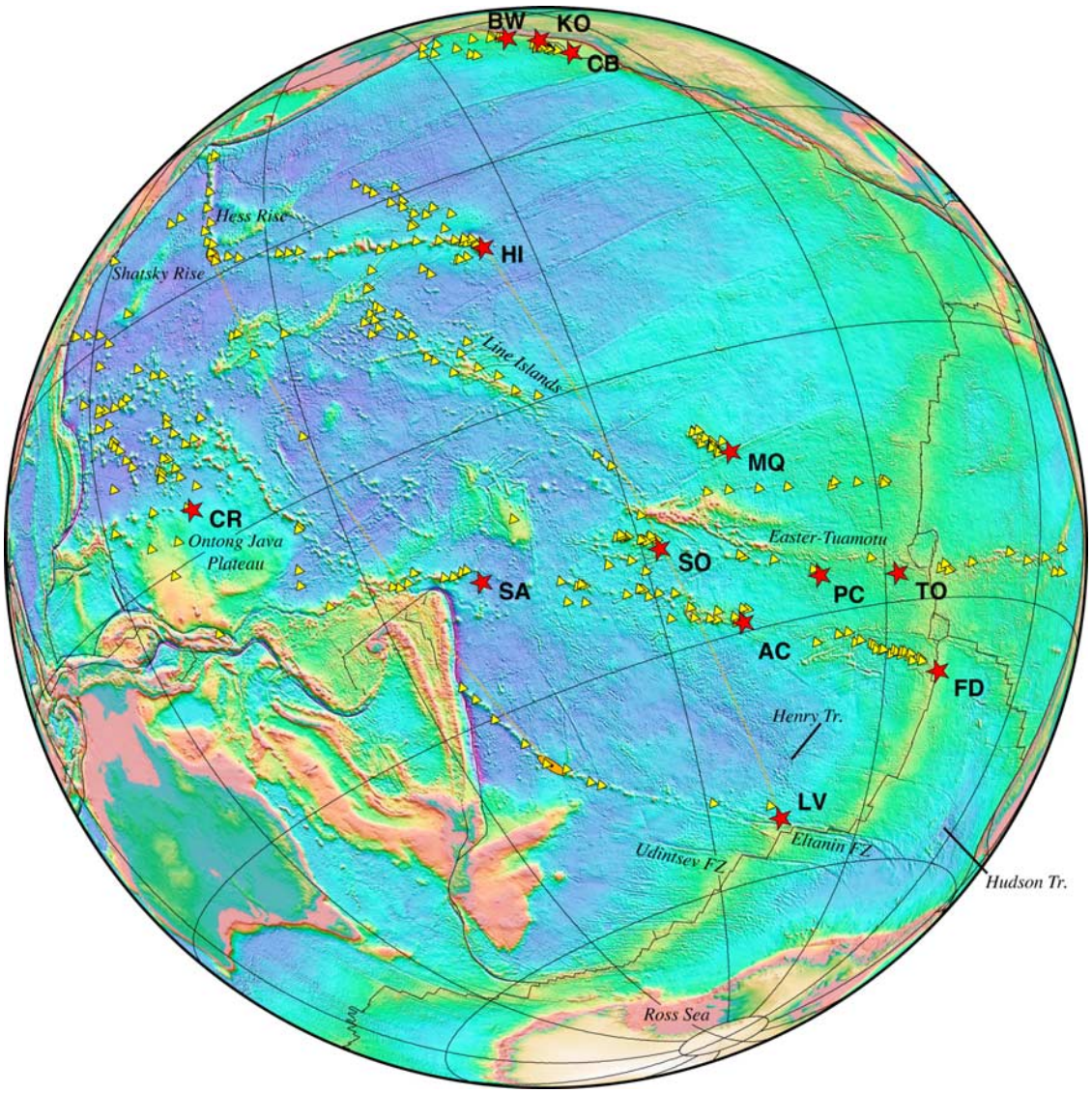

Figure 1. Pacific basin with active (or recently active) hot spots (red stars) and all available samples (yellow triangles) for which $^{39}Ar/^{40}Ar$ ages have been determined [*Clouard and Bonneville*, 2005]. Orange error ellipse describes possible locations of Hawaii-Emperor and Louisville chain bends at ~48 Ma with dashed line indicating the corresponding great circle separation (constant through time for fixed hot spot models). Abbreviations are HI, Hawaii; LV, Louisville; FD, Foundation; PC, Pitcairn; CR, Caroline; CB, Cobb; MQ, Marquesas; SA, Samoa; KO, Kodiak; BW, Bowie; AC, Austral-Cook; SO, Society Islands; and TO, Tuamotu.

a change in plume drift and that no APM motion change was needed [*Tarduno et al.*, 2003]. Nevertheless, many interior sites on the Pacific plate have morphological features reflecting past tectonic events that collectively require a change in APM contemporaneously with the formation of the HEB. For example, major triple junction reorganizations took place in the South Pacific as Pacific-Antarctic spreading propagated northward, eventually intersecting the Pacific-Farallon ridge, which terminated spreading at the Pacific-Aluk ridge at ~Chron 21 and left the conjugate scars of the Henry and Hudson troughs (Figure 1) [e.g., *Cande et al.*, 1982; *Cande and Haxby*, 1991]. We note that the earliest arc volcanism at 48–51 Ma followed the initiation of Izu-Bonin-Mariana subduction in the western Pacific [e.g., *Cosca et al.*, 1998], and the recent redating of the HEB to 47–50 Ma [*Sharp and Clague*, 2006] greatly improves the correlation between these two events. Finally, it is now emerging that a HEB-like change in relative plate motion (RPM) between Australia and Antarctica took place at this time as well [*Whittaker et al.*, 2007]. Thus, the tectonic evidence suggest a large change in Pacific APM at the time of the HEB formation. While the paleomagnetic evidence may still imply a component of plume drift, it is becoming evident that the HEB event is tied to a predominantly global Eocene plate kinematic event [e.g., *Rona and Richardson*, 1978]. This realization increases the likelihood that some of the paleomagnetic anomalies could instead be caused by true polar wander [e.g., *Andrews*, 1985].

[4] While the HEB change is of primary concern, researchers have also proposed second-order changes in

Pacific APM to account for smaller kinks in Pacific hot spot trails [e.g., *Cox and Engebretson*, 1985; *Duncan et al.*, 1985; *Kamp*, 1991; *Lonsdale*, 1988; *Pollitz*, 1986; *Wessel and Kroenke*, 1997]. As is the case for the HEB, others have suggested such kinks simply reflect hot spot movement [e.g., *Cox*, 1999; *Koppers et al.*, 2001; *Norton*, 1995; *Steinberger*, 2000; *Tarduno and Cottrell*, 1997; *Tarduno et al.*, 2003]. If hot spots were fixed with respect to the mantle, then changes in APM may produce correlated kinks in colinear trails. Changes in Pacific APM would impact the tectonic regimes around the Pacific Rim, including changes in RPM, deformation along plate boundaries, changes in the direction and velocity of subduction, and changes in arc volcanism associated with these subduction zones. Often, boundary activity may actually be the cause of the APM change [e.g., *Lithgow-Bertelloni and Richards*, 1998]. Clearly, changes in Pacific APM should leave a distinct signature in the geologic record. The timing and sense of motion inferred by these tectonic events can then be correlated with the timing and direction of Pacific APM derived from hot spot trails. However, if the observed short-lived kinks were due to hot spot drift fluctuations alone, then one would not necessarily expect to find similar correlations with circum-Pacific tectonic events or even among copolar chains.

[5] One difficulty in assessing the suitability of fixed hot spot-derived APM models has been the lack of uncertainty estimates and the ability to detect shorter-lived APM excursions. We have recently developed a new hybrid method that can obtain continuous plate motion rotations and optimal hot spot locations with the assumption of a fixed hot spot reference frame, which we used to derive a new APM model for the Pacific since ~78 Ma [*Wessel et al.*, 2006]. However, if hot spot motions were significant during the early part of that interval, then our model may be biased for such ages. Unfortunately, as this APM model only extends to ~78 Ma it is not well suited to assess this potential shortcoming.

[6] To address this issue we present the first self-consistent, high-resolution APM models for the Pacific plate extending to the end of the Jurassic period (145 Ma). Two models were computed: (1) a smooth model in which the uncertainties in observed ages have been fully mapped into corresponding uncertainties in rotation opening angles, leading to a greater amount of averaging of rotations, and (2) a less filtered APM model in which minor (and short-lived) changes in APM still can be detected. Geometry and age data from 12 Pacific hot spot chains were used in the construction of these models. We interpret the models in the context of circum Pacific kinematic and magmatic events. Finally, we examine implications of the models for inter–hot spot distances, paleomagnetically derived latitudes, and the Pacific apparent polar wander path to determine whether fixed hot spot models may still serve a purpose in plate tectonic studies.

2. Modeling of Absolute Plate Motions

2.1. Pacific Seamount and Island Chains

[7] There are numerous hot spot trails on the Pacific plate (Figure 1). Not all hot spots have been active as long as the Hawaiian hot spot nor have they had the same consistent and voluminous delivery of magma to the surface. Many trails are poorly dated and some overlap and cross other trails. For those reasons only the clearest and best dated trails were used in our previous modeling [*Wessel et al.*, 2006]. In that study we focused on the Hawaiian-Emperor (HI), Louisville (LV), Foundation (FD), Cobb-Eickelberg (CB), Caroline (CR), and the Pitcairn-Gambier (PC) seamount chains and derived a self-consistent APM model back to ~78 Ma. As we now seek to extend our modeling further back in time, we must include older chains formed over hot spots that are now presumably extinct. For some of these chains their younger sections appear to overlap with the oldest Emperor stage and thus we have included the Musicians (MU), Liliuokalani and southern Shatsky Rise (SS), and the southern (SW) and northern (NW) overlapping trails traced through the Wake-Ratak-Gilbert-Ellice seamount groups. Finally, in order to extend our APM modeling back even further we chose to include the Mid-Pacific Mountains (MP) and the northern Shatsky Rise (SN) (Figure 2). While the origins of these two features remain poorly understood, they have both been suggested to involve hot spots erupting on or near a plate boundary [e.g., *Sager et al.*, 1999; *Winterer and Metzler*, 1984]. Although we will show that the geometry and age progression of both features can be reasonably well modeled as hot spot trails, enough questions [e.g., *Mahoney et al.*, 2005] remain to label this association preliminary and necessarily speculative. We believe a rigorous reassessment of plate rotations including these chains (in addition to the dominant Hawaii and Louisville trails) will better determine if fixed hot spot models are appropriate for the early Emperor interval and what shortcomings might be revealed in the process. Table 1 lists the optimal locations and circular uncertainties of all 12 hot spots used in our modeling efforts.

[8] We have excluded Neogene chains not believed to be hot spot related (such as the Puka-Puka chain [e.g., *Sandwell et al.*, 1995]), chains that appear to have a complex origin (e.g., the Tuamotu-Line Island connection, although originally included by *Morgan* [1972]), and chains whose dates lack a clear progression (such as Tuvalu [*Koppers and Staudigel*, 2005]). We also chose to leave out the several short, parallel trails of possible hot spot origin in the West Pacific Seamount Province where extensional volcanism may have played a significant role [*Koppers et al.*, 2003]. Finally, as we focus on the Cretaceous part of the Pacific plate motion we chose not to include the most recent short-lived trails in the central Pacific (e.g., Society, Marquesas, Austral-Cook, and Samoa) as their geometries and age progressions are generally well predicted by our existing model [*Wessel et al.*, 2006].

[9] One of the major problems in determining an APM model from hot spot-produced seamount trails lies in determining coeval segments on different trails used to fit copolar small circles. Because of the scarcity of radiometric dates, picking the end points of each segment based on chronology becomes very difficult. Furthermore, as segments become shorter, the uncertainty in their pole locations becomes very large. To avoid these obstacles, the polygonal finite rotation method (PFRM) [*Harada and Hamano*, 2000] and the hot spotting technique [*Wessel and Kroenke*, 1997] were recently combined into a hybrid technique

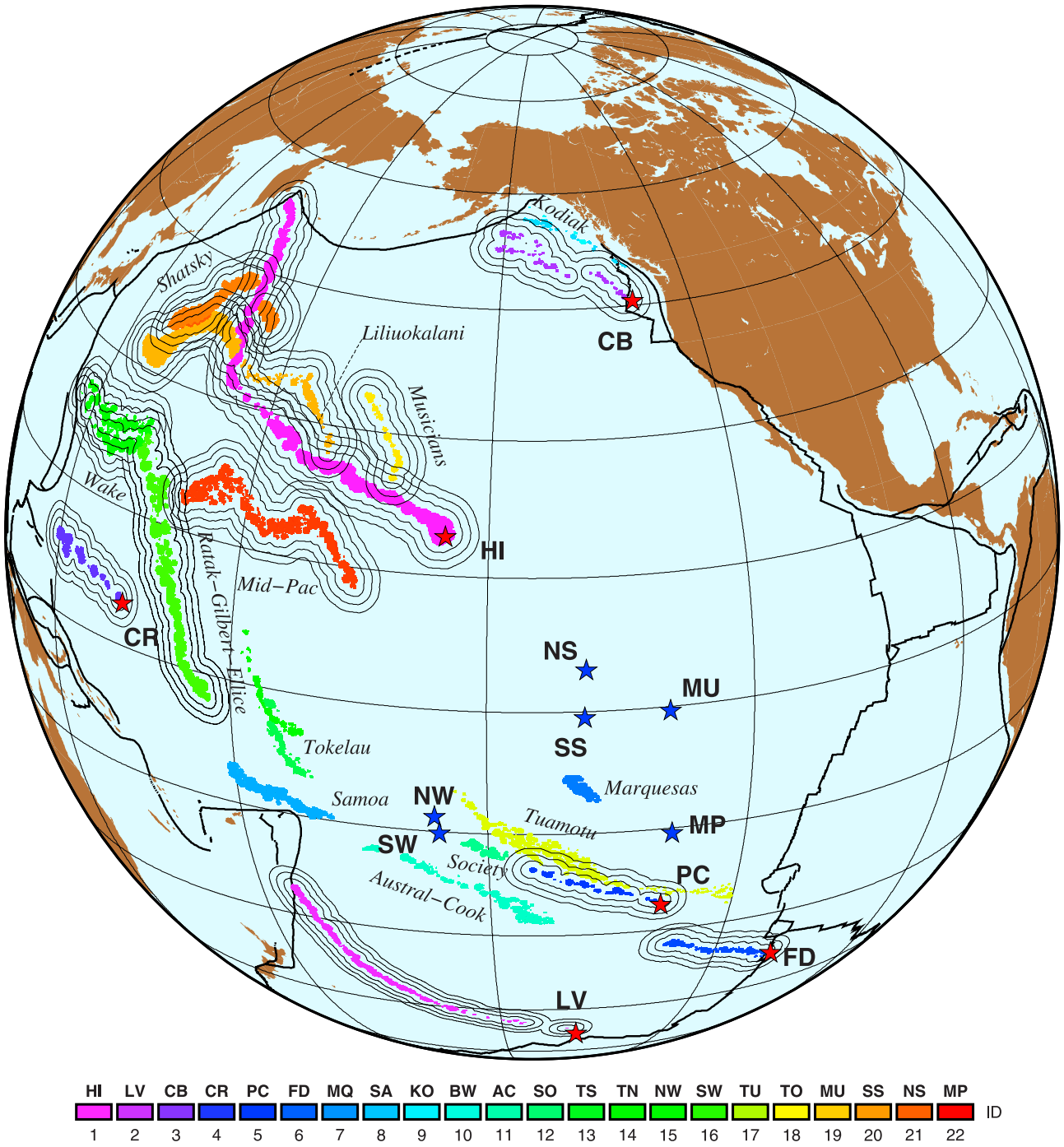

Figure 2. Seamount chain constraints based on the *Wessel* [2001] seamount database. Each chain has been assigned a unique ID (see legend). The polygon finite rotation method involves a grid search for all possible rotations (longitude, latitude, opening angle); only rotations that move current hot spot locations onto the corresponding chains (for at least two or more chains) are kept. We consider 12 chains, with six hot spots being recently active (red stars are HI, LV, FD, PC, CR, and CB; see Figure 1 for abbreviations) and the remaining 6 hot spots being extinct (blue stars are MP, Mid-Pacific Mountains; MU, Musicians; NW, northern Wake; SW, southern Wake; NS, northern Shatsky; SS, southern Shatsky). Chains not included in the modeling but used for testing predictions are MQ, SA, KO, BW, AC, SO, and TO (see Figure 1 caption). Distance contours (100 km interval) are shown for the included chains.

[*Wessel et al.*, 2006] and our APM modeling largely follows this methodology. Here, we will briefly review this procedure, referring to *Wessel et al.* [2006] for details.

2.2. Geometric Analysis

[10] We began by identifying the bathymetric expressions of all seamount and island chains for which radiometric dates are available. Bathymetry on a seamount-by-seamount

Table 1. Hot Spot Locations for WK08-G and WK08-A[a]

Tag	Name	θ	λ	r,[b] km
HI	Hawaii	19°12′N	155°03′W	25
LV	Louisville	52°24′S	137°12′W	75
FD	Foundation	37°54′S	110°00′W	25
PC	Pitcairn	25°54′S	129°15′W	25
CR	Caroline	4°48′N	163°39′E	50
CB	Cobb	45°33′N	129°15′W	75
NW	Wake north	13°06′S	156°00′W	50
SW	Wake south	15°15′S	155°30′W	50
MU	Musicians	0°30′S	129°45′W	50
SS	Shatsky south	2°00′S (00°45′S)	137°45′W (139°15′W)	50
NS	Shatsky north	3°49′N (04°43′N)	137°42′W (139°06′W)	50
MP	Mid-Pacific Mountains	16°40′S (15°40′S)	128°08′W (129°00′W)	50

[a]Same locations unless WK08-A values are given in parentheses.
[b]Prescribed radial uncertainty in hot spot location.

basis associated with each chain was given a unique ID number. As very few seamounts are present in the *Wessel* [2001] seamount compilation for the broad Shatsky plateau and trail, we augmented the seamount data with the outline of the high plateau by following the 4500 m bathymetric contour. In our revised method a bathymetric feature may have more than one ID number, allowing us to handle cases where hot spot chains cross or are so close that we cannot uniquely determine which chain a feature belongs to. In such cases the data may be required to constrain more than one chain at the same time. This improvement is the main adjustment that now allows us to extend our APM modeling further back in time. Figure 2 shows the various Pacific plate seamount chains that we have considered; not all were used directly in the modeling procedure. Specifically, the chains with distance contours were used to determine APM parameters whereas others were used to test the model predictions.

[11] Examining all possible rotation poles and opening angles, we retained only those rotations that successfully reconstructed the present hot spot locations onto the corresponding seamount chain (i.e., the projected point falls inside the distance contour given by the r values in Table 1). We tracked all possible combinations of hot spots that produced acceptable rotations; in particular, we wanted to find rotations that simultaneously fit as many chains as possible for a given opening angle. The number of chains used to determine a particular rotation varies with opening angle (and hence age). As in the work by *Wessel et al.* [2006], the initial average rotations were used to refine hot spot locations by applying the hot spotting method [*Wessel and Kroenke*, 1997]. This process was iteratively applied until convergence. It is this procedure that ensures that hot spot locations and rotation parameters are internally self-consistent. Figure 3 shows all rotations that satisfied our fit criteria; the link of white circles represents average rotations

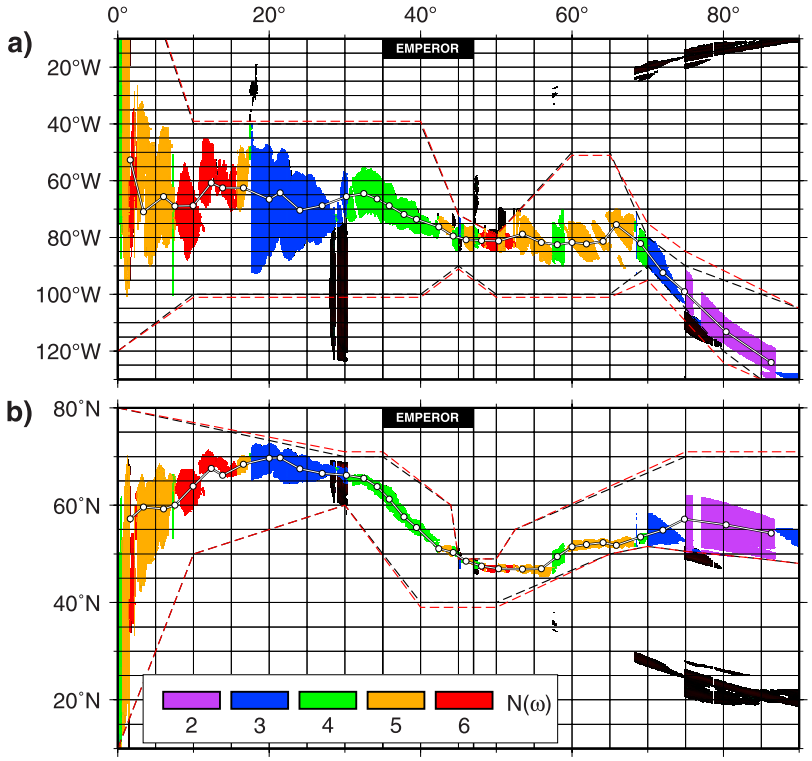

Figure 3. All possible rotation pole coordinates as functions of opening angle (ω), color coded by how many chains were fitted simultaneously (black means rotations were deemed unsuitable on closer inspection). Trial rotations outside the dashed red lines were excluded as they always failed to fit the trails. (a) Longitude of rotation poles. Line with white dots indicate smoothed model using the initial ~2° window for ω. (b) Same for rotation pole latitudes. These estimates form the geometric part of the WK08-G model. Vertical lines delineate the range of angles corresponding to the 60–90 Ma Emperor stage.

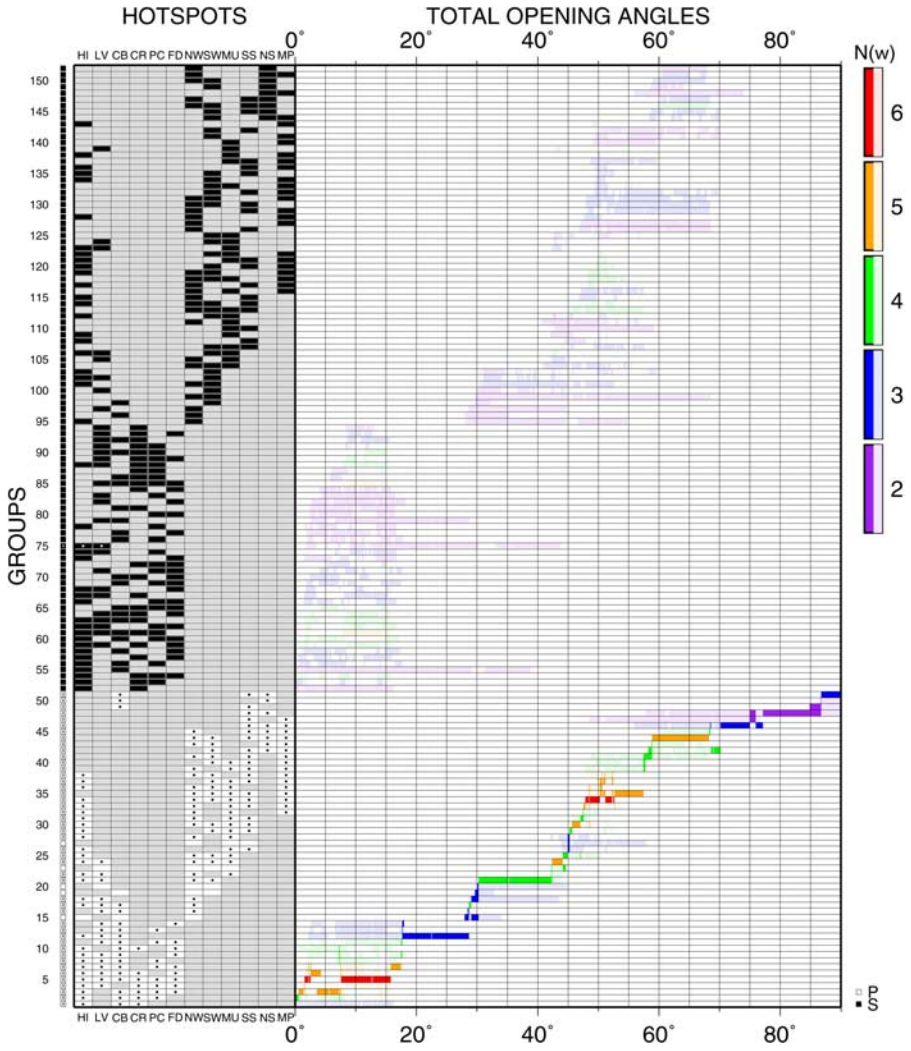

Figure 4. Summary of all 152 hot spot groups that produced acceptable rotations. For each opening angle, many combinations of chains produced rotations that fit two or more chains. The group with the largest number of chains for a given range of opening angles is called the primary group (white in left sidebar), all other combinations are secondary (black). The range of opening angles possible for any group is given in the main window, with primary groups in solid colors and secondary groups in faded colors. Check marks and black/white dots indicate groups used in the final rotation model; it includes almost all primary groups plus one secondary group (HI + LV; to stabilize the solution for opening angles when the primary group did not contain both of these chains). Five primary groups gave erratic rotations and were excluded.

derived from this population. Because the age ranges for the various chains do not all overlap, the maximum number of chains that can be fit for any given opening angle is six. As was the case with our previous model, the latitudes of the rotation poles seem better constrained than their longitudes; this is presumably a geometric consequence of chain orientation with respect to the coordinate system. However, for opening angles beyond $\sim 70^\circ$ the uncertainty increases considerably, reflecting the broad bathymetric trends that delineate the two Shatsky traces (see Figure 2).

[12] We also analyzed how groups of chains used to determine acceptable rotations vary with opening angles. Figure 4 presents a breakdown of how many chains were used to determine the rotations for a particular angle. For each opening angle, the maximum number of chains involved in determining a rotation, $N(\omega)$, is color coded; the corresponding group is called a primary group. Often, the make-up of a primary group stays constant over long, continuous ranges of opening angles. For instance, for the range $7.5-16^\circ$ a maximum of six chains would determine the rotation; these were always HI, LV, CB, CR, PC and FD. However, for the same angles, different but smaller groups would also produce acceptable rotations. The lighter colors indicate these secondary groups for the ranges of opening angles they apply to. While in this study we have only retained rotations from almost all primary groups (solid color trends) and the single secondary group of HI, LV for its long continuity, a more detailed study of the secondary groups may reveal how much influence a particular chain has on the solution for a particular range of opening angles.

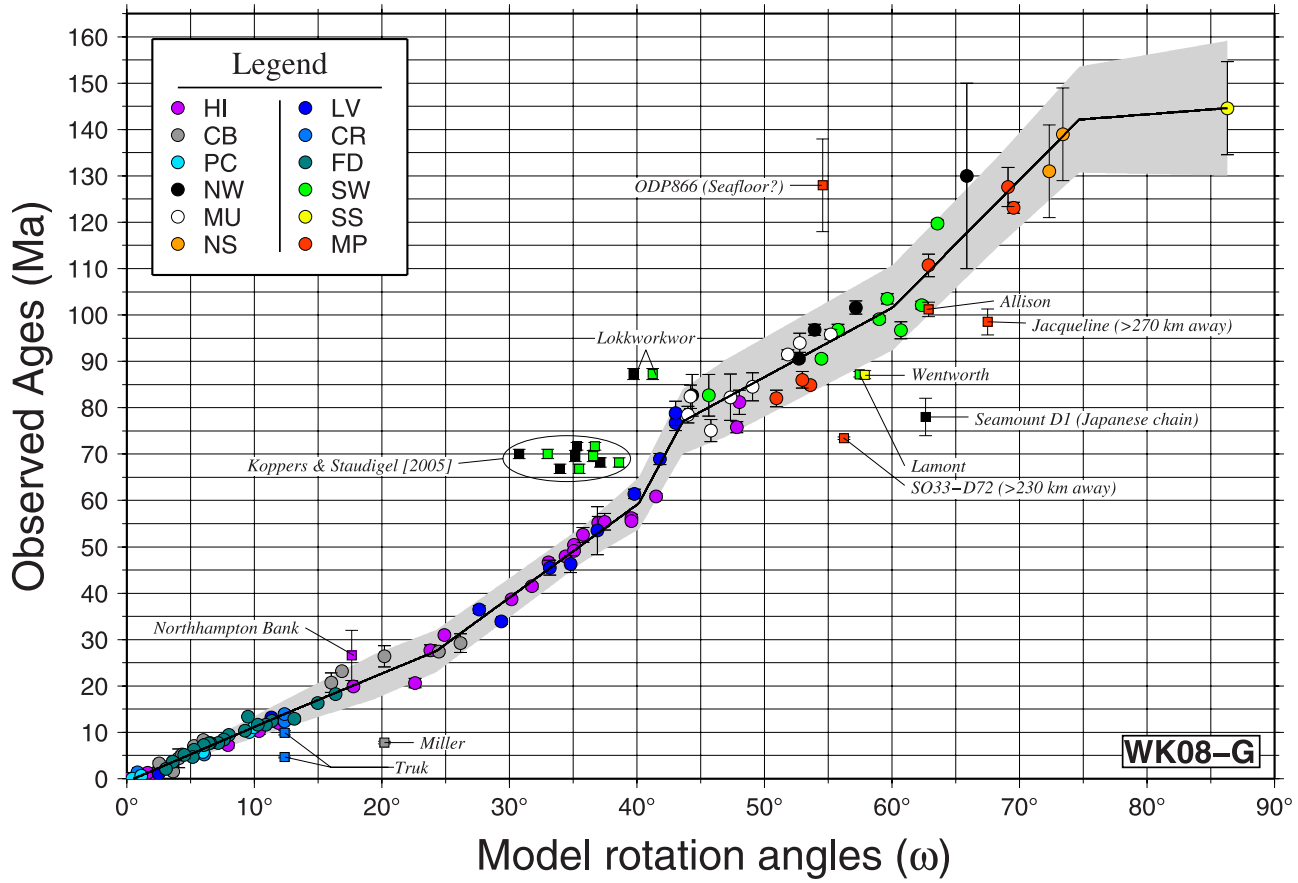

Figure 5. The $t(\omega)$ plot for the 12 Pacific chains used in the APM modeling with moderate smoothing (WK08-G). The linear spline found six significant segments back to 144 Ma. Gray band represents a 95% confidence level for the spline. Given these uncertainties from ages, we project them onto the opening angle (ω) axis to yield new ω windows to use for the smoothing of rotations (e.g., Figure 3). Circles represent samples used in the interpolation, whereas squares are samples rejected for reasons stated in the text. Some individual samples from the overlapping strands in the Ratak-Gilbert-Ellice chains appear twice (i.e., both as NW and SW with same age but different ω) as they could belong to either chain.

2.3. Temporal Analysis

[13] It has generally been established that intraplate volcanism may originate from a variety of sources, not all involving mantle plumes [e.g., *Epp*, 1984; *Foulger and Natland*, 2003; *Hieronymus and Bercovici*, 2000; *McNutt et al.*, 1997]. This fact makes it nontrivial to track hot spot-produced age progressions through mixed populations of seamounts. Our approach has thus been (1) to let the geometric analysis determine the likely paths of plate motion and (2) to examine all dated samples that locate within 300 km of these predicted trails. It is expected that some nonhot spot contamination will occur but the dominant signal should be the monotonically increasing age trend typical of hot spot trails. This is indeed what we find; the following paragraphs explain how we determine this trend and its uncertainty.

[14] Given the geometric information summarized by the average rotations (Figure 3), we regressed observed ages versus the model's predicted opening angles (Figure 5). Here, all available $^{40}Ar/^{39}Ar$ sample ages whose locations sit on flow lines that pass within 300 km of any hot spot were considered; these data were taken from the recent Pacific-wide age compilation of *Clouard and Bonneville* [2005] with revised ages from the Hawaii-Emperor [*Duncan and Keller*, 2004; *Sharp and Clague*, 2006], Louisville [*Koppers et al.*, 2004], and Ratak-Gilbert-Ellice [*Koppers et al.*, 2003] chains as well as the Shatsky plateau [*Mahoney et al.*, 2005]. We examined this relationship and made the following interpretations:

[15] 1. A few dated seamounts from chains with fairly well developed age progressions appear to be incompatible with the overall trend. For instance, in the Hawaiian chain a single sample from Northampton Bank appears >5 Myr older than other samples of similar angular distance; it also has a large individual age uncertainty. Likewise, in the Caroline chain there are several different ages reported for the Island of Chuk (Truk), and the two youngest do not fit the overall age progression trend. Our solution was to only keep the two oldest dates. For the Cobb chain it is similarly known that Miller seamount is associated with both a young (7.8 Ma) and old (26.4 Ma) age, and again the young date does not fit the overall trend. On the basis of geochronology and petrology, *Dalrymple et al.* [1987] concluded that Miller was constructed on young crust, probably near a

spreading ridge, hence the older age seems more appropriate. In all these cases we excluded the outlying points.

[16] 2. For the older chains we found questionable values as well. For instance, the database lists ODP 866 as a sample belonging to the Mid-Pacific Mountains. However, this age is >34 Ma older than the overall trend, yet almost exactly matches the predicted seafloor age [*Müller et al.*, 1997]. We thus disregarded this data point as a seafloor sample. Others, such as the Jacqueline and SO33-D72 samples are both over 250 km removed from the optimal track and were excluded on those grounds. At Allison we found two conflicting sample ages. Following *Pringle and Duncan* [1995], we excluded the younger age on the grounds that it had most likely been disturbed and thus did not give an accurate estimate of the crystallization age. Other discordant sample ages were not as easy to neither explain nor justify their omission. For instance, seamount D1 locates within the Wake Islands but is listed in the catalog as belonging to the Japanese Seamounts chain. Wentworth, Lamont, and Lokkworkwor all have ages that differ from other seamounts of similar angular position. Finally, the recent samples from *Koppers and Staudigel* [2005] do not fit the age trend established without these samples. This outlying group (circled in Figure 5) exhibits more or less constant ages, possibly reflecting nonhot spot activity related to secondary extentional magnetism following changes in APM [e.g., *Koppers and Staudigel*, 2005; *Koppers et al.*, 2007; *Sager and Keating*, 1984; *Wessel and Kroenke*, 2007].

[17] With these few outliers removed, we fitted a piecewise linear spline to the remaining data points. Starting with a single segment, the spline routine added additional segments until the extra parameters did not significantly improve the fit. The knot points were automatically adjusted to minimize the misfit. The gray band (Figure 5) indicates the 95% level of confidence for the spline. It is clear that the uncertainty in the relationship between age and opening angle increases with age. This trend reflects a variety of conditions, such as larger intrinsic uncertainties in the analytic ages for older, more altered samples, greater uncertainty in assigning a particular seamount to its hot spot, and increased possibility of a sample being contaminated by rejuvenated or extentional volcanism. By combining the age-angle relationship (Figure 5) with the geometric rotation parameters (Figure 3) we obtain a minimally smoothed APM model named WK08-G; it retains more geometric correlations among chains due to the lower amount of filtering. Covariance estimates for the kth rotation are given by

$$C_k = \mathrm{Cov}(\mathbf{r}_k) = \frac{1}{\hat{k}_k}\begin{bmatrix} a_k & b_k & d_k \\ b_k & c_k & e_k \\ d_k & e_k & f_k \end{bmatrix} g_k \qquad (1)$$

with parameters listed in Table 2; the uncertainties in rotation pole locations are displayed in Figure 6. We also show the range of possible opening angles within each pole location's confidence region by contouring the upper and lower limits on the angle separately [e.g., *Chang*, 1987]. However, our contours have the mean opening angle removed, thus showing deviations from the mean.

[18] The smoothing of rotations (e.g., Figure 3) is initially somewhat arbitrary but intended to reflect the typical width of seamount chains [*Harada and Hamano*, 2000; *Wessel et al.*, 2006]. Once the initial relationship between angles and ages (Figure 5) has been determined, however, we used the uncertainty band on this relationship to map age uncertainties into the corresponding angle uncertainties (Figure 7). This yielded the more heavily filtered APM model WK08-A that in some regards is less desirable as many of the secondary changes in APM have been filtered out. However, on the other hand, the rotations for a particular age now have more realistic uncertainties. We find both models have uses in the analysis of the tectonic origins of these APM changes. Table 3 lists the parameters for the WK08-A model.

3. Results

3.1. Assessment of the WK08-A and WK08-G Models

[19] The WK08-A APM model allows us to backtrack all dated samples to their point of origin (i.e., presumably the corresponding hot spot). Furthermore, we can use the APM model to assign a predicted age to any bathymetric feature that does not have an observed age. Such points can then be backtracked to their point of origin and used to assess model misfit (mostly in the across-track direction). By mapping all points to a common reference frame we may examine how well the WK08-A model fits both the geometric and radiometric data (Figure 8). The two populations (red for observed and green for predicted seamounts ages) can be approximated by elliptical distributions. For comparison, the corresponding results for our previous model (<78 Ma only) are shown as dashed lines. Clearly, incorporating the more vaguely defined older chains has broadened the model misfit to both geometry and ages. For the present model, the across-track misfit is now exceeding 100 km.

[20] The predicted trails of the less filtered WK08-G model are shown in Figure 9, with uncertainty ellipses at all reconstructed points. Here, solid lines (with red reconstructed points) indicate the best fit for chains included in the modeling, whereas open lines (with white reconstructed points) indicate predictions for Pacific chains not contributing to the model. In general, this APM model fits both types of chains well, but there is obviously uncertainty in assigning seamounts to a particular chain among the many Austral-Cook lineaments. Historically, several hot spot trails have been proposed for this region [e.g., *Bonneville et al.*, 2002; *Dickinson*, 1998; *McNutt et al.*, 1997; *Turner and Jarrard*, 1982]. Here, we simply show a possible alignment from the Macdonald hot spot which tracks through the Tuvalu chains, as suggested by *Koppers and Staudigel* [2005].

[21] Similarly, Figure 10 shows the predicted trails for the smooth WK08-A model for each of the 12 hot spots. One difference between the two models is the larger number of rotations (and hence reconstructed points) in the WK08-G model due to the narrower filter windows. Being less filtered means the WK08-G model retains some of the second-order APM changes that can be clearly identified in some chains but not so clearly in others; this is partly a geometric effect. It is beyond the scope of this paper to assess all possible correlations (or lack thereof) between

Table 2. WK08-G Finite Rotations and Their Covariance Matrices[a]

θ	λ	t	ω	a	b	c	d	e	f
57°10′N	52°43′W	1.31	1.66	1.162	−0.209	4.058	1.790	−5.215	11.98
59°39′N	70°55′W	3.36	3.40	3.291	−0.656	2.157	0.770	−1.560	2.448
59°13′N	65°37′W	6.48	6.04	3.655	−0.871	3.643	2.494	−4.934	9.388
60°03′N	68°55′W	8.27	7.55	3.760	1.317	2.823	−0.111	−1.436	5.458
63°52′N	68°49′W	11.11	9.96	2.540	1.255	3.158	0.764	−1.906	6.655
67°35′N	60°48′W	13.95	12.4	4.210	−0.166	10.67	0.754	−2.967	4.682
66°09′N	62°33′W	15.67	13.9	5.952	3.223	10.35	0.993	−2.362	10.12
68°26′N	62°34′W	18.76	16.6	27.49	24.17	28.30	−20.88	−22.09	42.11
69°39′N	66°33′W	22.66	20.0	21.01	9.957	6.432	6.909	2.107	11.68
69°45′N	64°14′W	24.35	21.5	40.08	37.34	38.67	−4.233	−4.700	3.070
67°31′N	70°26′W	27.28	24.0	11.58	4.064	5.218	6.883	0.522	8.430
66°32′N	68°45′W	33.00	27.0	5.986	0.270	5.699	1.459	−5.516	10.04
66°10′N	65°37′W	39.44	30.2	3.350	0.823	1.808	−0.262	−0.225	0.635
65°33′N	64°31′W	44.08	32.5	6.864	−1.126	1.056	1.785	−1.564	3.686
63°48′N	66°20′W	47.56	34.3	9.239	7.794	18.08	−3.291	−7.688	5.482
61°16′N	68°46′W	50.8	35.9	11.25	12.35	30.63	−0.783	−3.625	2.292
57°34′N	71°52′W	54.7	37.8	6.260	1.697	18.73	0.931	−4.621	3.095
55°23′N	73°33′W	58.0	39.5	9.386	8.043	16.21	−1.139	−2.720	1.474
51°05′N	76°19′W	71.0	42.4	5.608	2.745	14.69	−0.801	−2.054	1.500
50°18′N	79°27′W	78.1	44.3	16.72	3.810	4.337	−9.382	−2.296	6.105
48°29′N	80°44′W	80.6	46.0	49.13	−1.608	6.815	−28.83	−1.148	18.28
47°29′N	81°01′W	83.7	48.0	54.36	−4.277	7.956	−8.499	−4.629	5.870
46°55′N	81°14′W	87.1	50.3	52.57	−6.814	4.439	−13.18	−1.476	6.846
46°53′N	78°44′W	91.7	53.4	63.63	−9.687	15.01	−12.70	−10.85	16.54
46°57′N	81°44′W	95.5	56.0	77.19	4.299	0.998	8.084	−2.073	20.78
49°25′N	82°32′W	98.6	58.1	21.59	−0.759	5.341	−7.478	10.60	28.31
51°27′N	81°44′W	101.6	60.0	78.50	−21.54	7.674	−16.79	4.593	18.10
51°58′N	82°14′W	106.8	61.9	53.86	−20.73	11.13	−15.33	3.063	13.76
52°17′N	81°20′W	112.8	64.1	36.65	−9.630	5.362	−22.92	5.565	16.45
51°47′N	75°27′W	117.7	65.9	183.5	−75.27	36.56	−107.3	42.06	72.56
53°30′N	82°05′W	126.5	69.0	284.6	−51.81	21.16	−140.4	43.94	116.9
54°51′N	92°27′W	134.6	72.0	234.1	102.5	91.90	92.93	92.21	111.6
57°07′N	99°06′W	142.2	74.9	344.5	74.83	147.2	0.813	136.5	162.1
56°00′N	113°09′W	143.3	80.4	389.5	−49.77	146.3	−162.6	191.1	313.8
54°16′N	124°03′W	144.6	86.3	102.9	−6.339	44.29	7.751	41.24	59.25

[a]Opening angle ω is in degrees, and t is in Ma. The covariance matrix for each rotation $\boldsymbol{R}$ is defined in equation (1), with a–f given in rad^2, $g = 10^{-5}$, and k set to 1.

predictions of our APM model and observed tectonic and magmatic circum-Pacific events; this is the topic of another manuscript (L. W. Kroenke et al., manuscript in preparation, 2008). However, we will briefly address four apparent APM changes (red arrows) highlighted in Figure 9. The most prominent (1; at ~48 Ma) is the HEB change already mentioned, being possibly a response to major tectonic events further west, such as the India-Eurasia collision [e.g., *Patriat and Achache*, 1984] and the initiation of the IBM subduction zone [e.g., *Cosca et al.*, 1998]. These and other events in the Chron 22-21 timeframe appear to correlate remarkably well with the change in APM. However, it is also likely that such a large event could affect mantle flow and hence plume motions [*Whittaker et al.*, 2007]. The next change (2; at 28–24 Ma) might correlate with the breakup of the Farallon plate [e.g., *Handschumacher*, 1976; *Hey*, 1977; *Lonsdale and Klitgord*, 1978]. A short-lived northward jog in both the Hawaii and Louisville chains were noted by *Lonsdale* [1988] and later also identified in the Gulf of Alaska [e.g., *Wessel and Kroenke*, 1998; *Wessel et al.*, 2006]. The next change (3; at 17–14 Ma) correlates with numerous tectonic events around the Pacific, including subduction of the Marcus-Necker ridge [e.g., *Miller et al.*, 2006], rapid extension in the Basin and Range province [e.g., *Dilles and Gans*, 1995], and transrotation in the Los Angeles Basin [e.g., *Ingersoll and Rumelhart*, 1999], yet the primary cause has not been identified. Finally, the last event (4; at ~6 Ma) involves a recent APM change noted by many investigators [e.g., *Andrews et al.*, 2006; *Epp*, 1984; *Wessel and Kroenke*, 1997]. Proposed causes of this APM change range from slab detachment [*Cox and Engebretson*, 1985] to an intensifying collision between Ontong Java and the Australia plate margin [*Wessel and Kroenke*, 2000, 2007]. Note that while the age analyses (Figures 5 and 7) clearly indicate a significant change in opening rate around 30–35 Ma, no corresponding significant geometric change was determined. This timeframe corresponds to a section of the Hawaii chain ($\omega \sim 25$–$35°$) where its bathymetric expression is sparse and subdued, yielding fewer rotations to process (Figure 3).

[22] Geometrically, the models based on fixed hot spots have always been acceptable, as shown in earlier works [e.g., *Harada and Hamano*, 2000; *Wessel et al.*, 2006]. In particular, with only the Hawaii-Emperor and Louisville chains constraining the oldest Emperor stage, it is possible to determine rotations that will predict an almost perfect trail through the middle of the data, and with less filtering the more detailed the fit. However, once ages are considered it appears that a discrepancy exists between the temporal information provided by the two chains. *Wessel et al.* [2006] found that the latest redating of Emperor seamounts (making them younger) and Louisville seamounts (making them older) led to a poorer fit than previously determined for this section [see also *Koppers et al.*, 2004]; thus geometry is

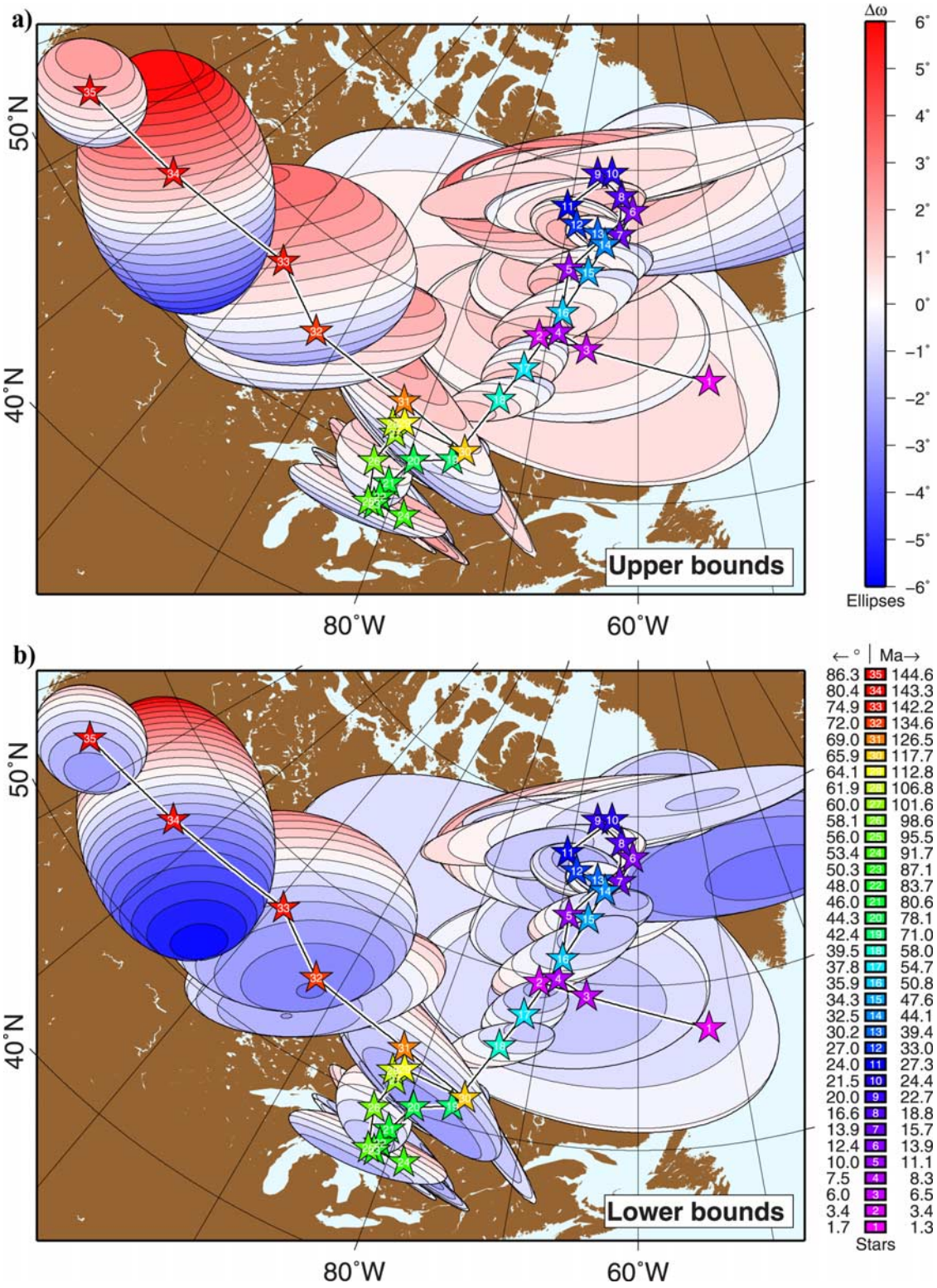

Figure 6. Rotation poles and their confidence regions for the geometric Pacific APM model WK08-G (also see Table 2). For the three youngest rotation poles the large error ellipses are not plotted. Numbered stars indicate locations of rotation poles, with colors reflecting opening angle and age. (a) Lower surface of opening angle deviations from mean value. (b) Same for upper surface of opening angles (see text for details).

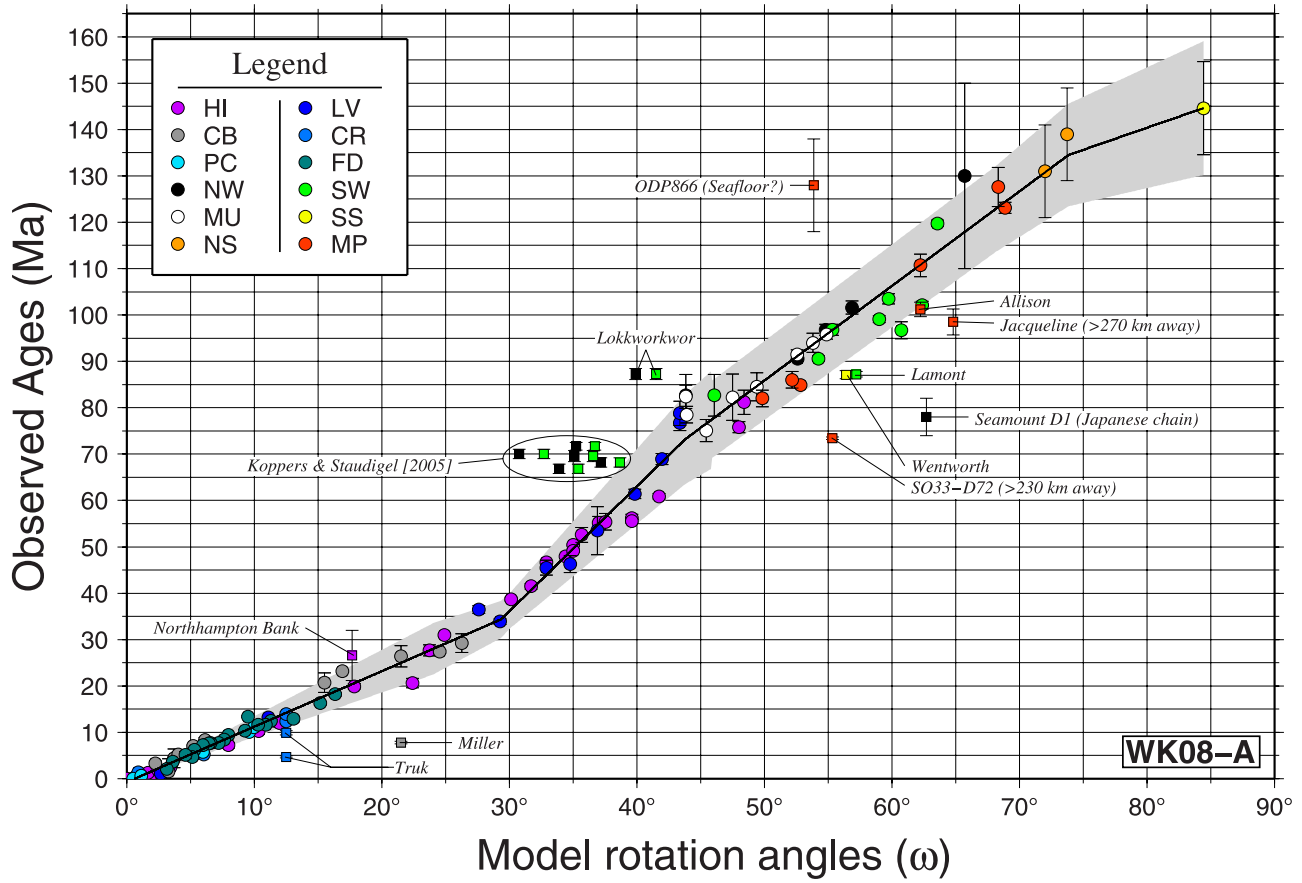

Figure 7. The $t(\omega)$ plot for the 12 Pacific chains used in the APM modeling with appropriate smoothing that reflects age uncertainties (WK08-A). Here, the linear spline found four significant segments back to 144 Ma. See Figure 5 for details.

only part of the solution [e.g., *Koppers et al.*, 2007]. The APM models developed here differ in that several additional chains have been included to better define the APM for the critical early Emperor stage. Figures 3 and 10 show that the geometries of these three to five trails are congruent and this has produced a very tight fit to the geometry. The age progressions determined in Figures 5 and 7 appear to provide confirmation that APM modeling of hot spot trails

Table 3. WK08-A Finite Rotations and Their Covariance Matrices[a]

θ	λ	t	ω	a	b	c	d	e	f
49°18′N	49°30′W	0.78	1.02	1.148	0.602	3.372	0.672	−1.079	3.554
53°43′N	56°53′W	2.58	2.66	2.370	0.199	2.888	3.080	−1.248	9.308
59°39′N	66°03′W	5.89	5.39	5.492	0.625	5.323	4.549	−3.032	14.85
62°52′N	70°52′W	8.86	8.23	6.238	3.365	10.19	0.591	−12.59	33.88
65°22′N	68°41′W	12.29	10.3	13.44	5.678	5.151	18.57	7.154	38.73
68°15′N	61°32′W	17.47	15.5	13.62	6.050	10.14	−0.263	−15.96	59.87
68°47′N	69°50′W	24.06	20.4	34.08	5.899	30.85	6.142	−38.03	77.96
67°43′N	70°48′W	28.28	23.6	29.04	5.501	27.98	5.904	−32.30	65.30
66°34′N	68°44′W	33.54	27.7	47.83	−28.36	42.46	54.51	−70.51	132.1
65°26′N	64°15′W	40.10	31.6	24.09	−7.689	14.18	8.881	−18.42	30.25
63°01′N	66°41′W	47.91	34.6	26.50	15.33	53.24	−10.04	−26.08	18.44
60°36′N	69°40′W	53.35	36.1	26.48	22.57	95.39	−7.216	−20.64	8.901
56°56′N	72°56′W	61.1	38.4	25.03	21.90	80.09	−9.575	−23.07	11.21
50°02′N	78°21′W	74.5	44.0	42.11	64.57	258.6	−35.70	−91.87	42.63
47°18′N	82°06′W	83.5	48.8	55.90	−17.94	172.7	−7.560	−105.1	83.44
46°54′N	82°41′W	95.0	54.1	85.30	−1.472	8.837	−37.40	−5.179	25.94
51°19′N	85°07′W	106.2	60.1	153.6	−24.46	10.61	−1.655	1.610	52.73
52°10′N	85°48′W	112.3	62.4	87.02	−35.77	20.31	−18.29	3.921	23.06
52°32′N	80°20′W	118.4	66.5	85.88	−29.94	16.82	−58.07	16.81	52.64
54°08′N	88°11′W	125.0	69.6	285.7	−59.74	45.96	−190.5	91.76	250.6
56°13′N	112°15′W	131.9	78.6	516.5	−30.50	149.4	−148.8	191.0	320.5
54°26′N	123°34′W	144.0	84.4	258.7	−26.81	114.9	−41.46	135.3	200.7

[a]See Table 2 for more information.

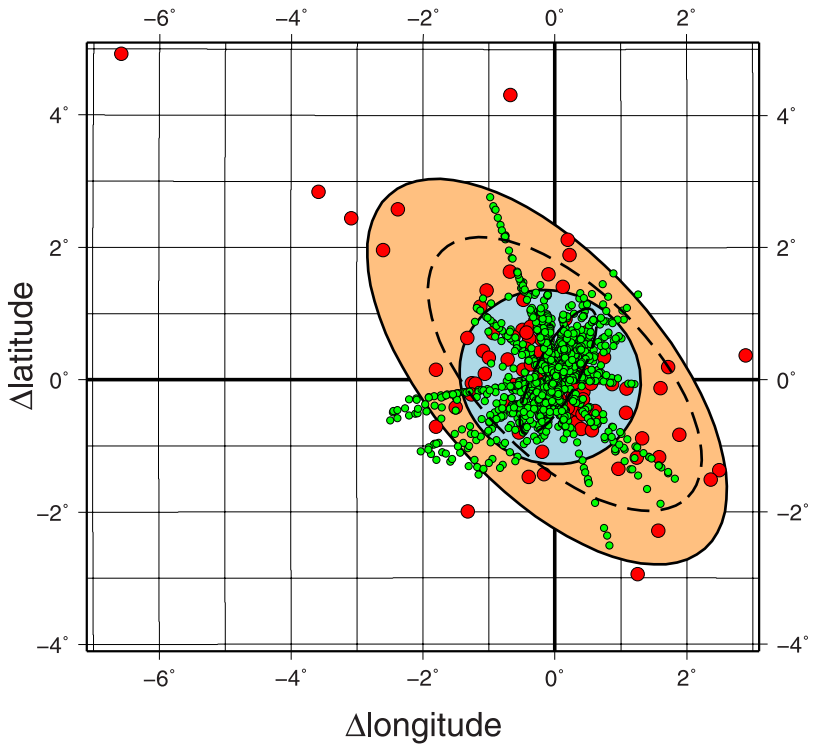

Figure 8. Scatterplot of all backtracked dated (red) and undated (green) seamounts for all 12 chains, referred to a common origin at (0°, 0°). Orange and blue ellipses indicate the corresponding 95% confidence regions on these two distributions, while dashed lines indicate the corresponding confidence regions for our previous ~78 Ma APM model [*Wessel et al.*, 2006]. The older chains, being both more diffuse and poorly dated, contribute significantly to the larger uncertainties.

can be extended back in time by considering overlapping trails. The uncertainty in ages and opening angles do not look much larger for the 60–90 Ma range than the ranges just before or after. Figure 11 further examines the quality of the age progression in the WK08-A APM model. Here, $\Delta t(t)$ is the difference between observed and predicted ages for all trails. As mentioned earlier, the scatter increases with age. The left box-and-whisker diagram, suggesting half of the values are within ±1 Ma, summarizes the distribution of Δt. Since age dating of older and altered rocks generally has larger uncertainties we also examine how the model age misfit to age ratio varies with age. That is, if instead the uncertainty is expressed as the ratio $\Delta t(t)/t$ (in percent), then the right box-and-whisker diagram shows a typical uncertainty of ±5%; extreme values occur for small values of t in the denominator. Given what is known about the duration of volcanic construction at seamounts and volcanic islands and the longevity of continuous and episodic eruptions in the same location [e.g., *Clague and Dalrymple*, 1989; *Koppers et al.*, 2003; *Moore et al.*, 1996; *Pringle et al.*, 1991], it seems to us that the geometric and temporal fit afforded by our APM models is, in general, a validation of the fixed hot spot hypothesis for the Pacific, but with the following caveats: (1) Our geometric and chronologic analysis is incapable of detecting any coherent motion of the Pacific hot spot group should such motion have occurred, (2) within the uncertainties of the analysis, relative hot spot motions, if present, seem unlikely to exceed ~5% of plate motions, and (3) this view does not address the complimentary information provided by paleomagnetics. Thus, our limits on motion within the Pacific hot spot group appear compatible with the results of Steinberger [e.g., *Steinberger*, 2000].

3.2. Assessment of Hot Spot Drift

[23] *Wessel et al.* [2006] introduced a novel map projection, called the plate tectonic projection, which reconstructs seafloor such that all flow lines become parallel. For hot spot chains this means the hot spot becomes the origin of the projection and the predicted hot spot trail is the horizontal model time axis. The coordinate axis normal to model time is the across-trail distance in degrees. Figure 12 shows reconstructed seafloor in the vicinity of the Hawaii (Figure 12a) and Louisville (Figure 12c) trails. In both cases the seamount trails are approximately horizontal and contained within the ±75 km band (horizontal dashed lines). Dated samples (yellow triangles) are plotted at their locations. Hot spot drift, if present, should leave behind evidence in the form of changing paleolatitudes, and indeed that is what has been inferred along the Emperor chain [e.g., *Tarduno and Cottrell*, 1997]. Unfortunately, similar observations are not yet available for the Louisville chain. However, unless both the Hawaii and Louisville hot spots moved so as to maintain a constant separation then their separation should vary with time. This separation can be assessed directly by estimating distances between samples of similar age from the two chains (Figure 12b). Here, groups of Hawaii and Louisville rock samples with compa-

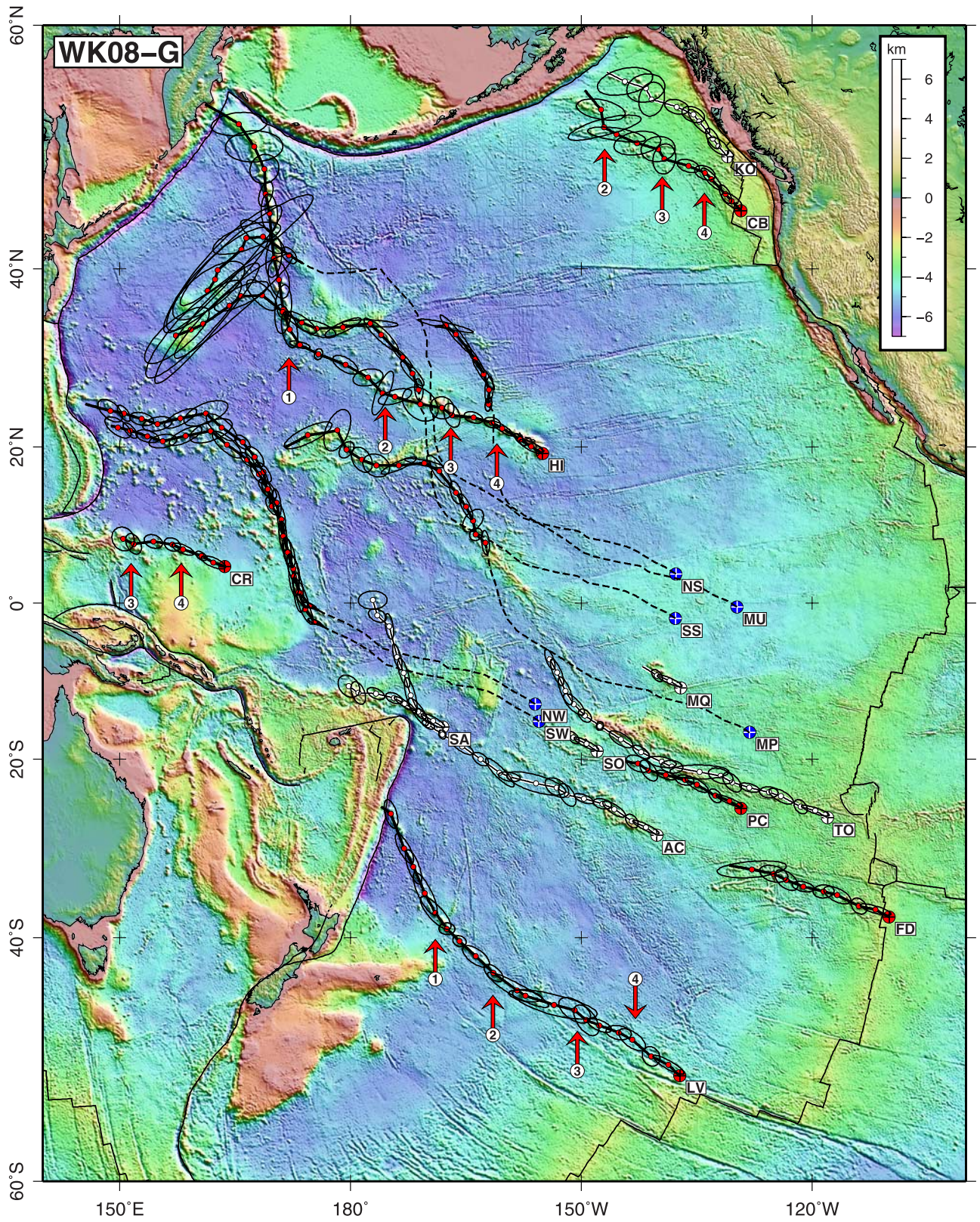

Figure 9. Pacific plate with predicted tracks and 95% confidence ellipses on reconstructed points (red and white) along each trail for the WK08-G APM model. Solid black lines (and red points) are used for trails that constrained the model, with open lines (and white points) for prediction at other trails. Red (blue) circles indicate the model locations of active (extinct) hot spots; white circles show other hot spots not used in determining the APM. Long dashed lines connect extinct hot spots with assumed seamount chain. Red arrows highlight changes in APM thought to reflect tectonic events at the plate perimeter (see text).

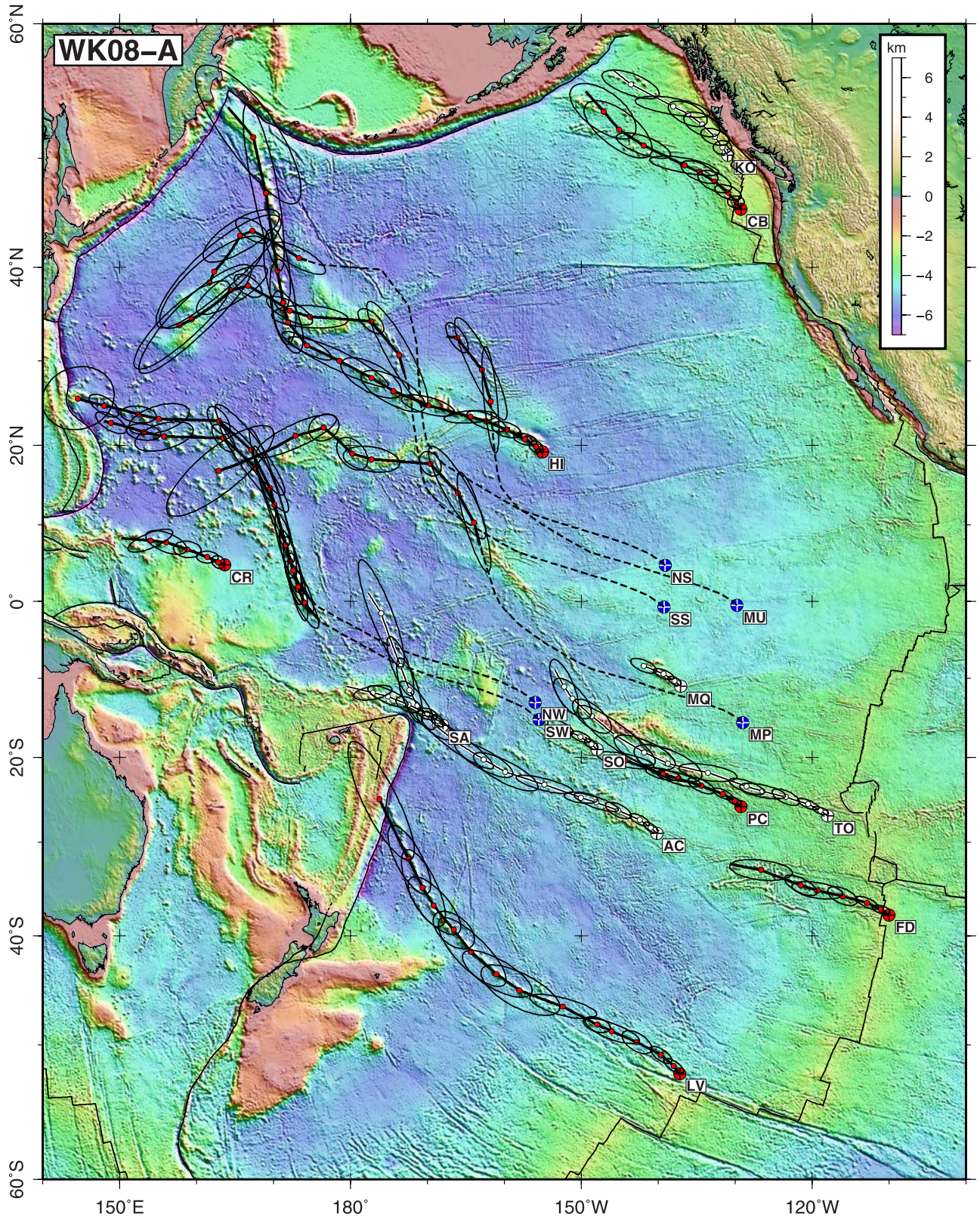

Figure 10. Predictions of WK08-A, a smooth APM model for the Pacific. The secondary APM changes seen in Figure 9 are no longer pronounced or have been smoothed out completely.

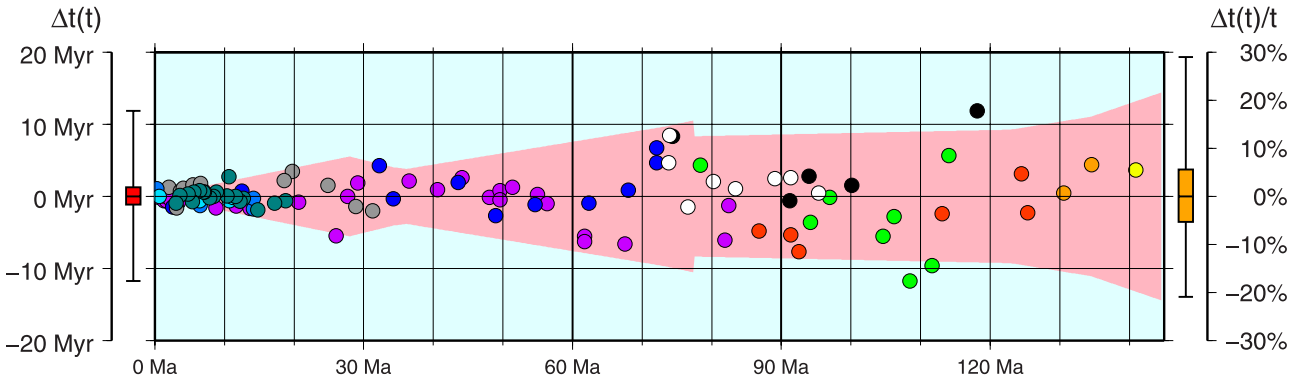

Figure 11. Difference between observed and predicted ages, $\Delta t(t)$, versus predicted age, t, for all 12 chains (see Figure 5 caption for symbol color code). Light red band indicates 95% confidence level. Red box-and-whisker diagram (horizontal bars indicate minimum, 25% quartile, median, 75% quartile, and maximum value) summarizes the $\Delta t(t)$ population, whereas the orange diagram shows the distribution after normalizing $\Delta t(t)$ by t.

rable ages (see yellow tie lines for groups) were used to calculate all possible intersample distances. These distances were then reduced by the expected fixed inter–hot spot separation as estimated from the observed HEB and LV bend separation (72.61 ± 1.10°) by *Wessel et al.* [2006] (see Figure 1). The notched box-and-whisker diagrams summarize $\Delta(t)$, the populations of deviations from the expected separation (yellow dots). We find that the available data up to ~55 Ma is clearly showing no significant variations with age. However, for the critical earlier ages we start to see

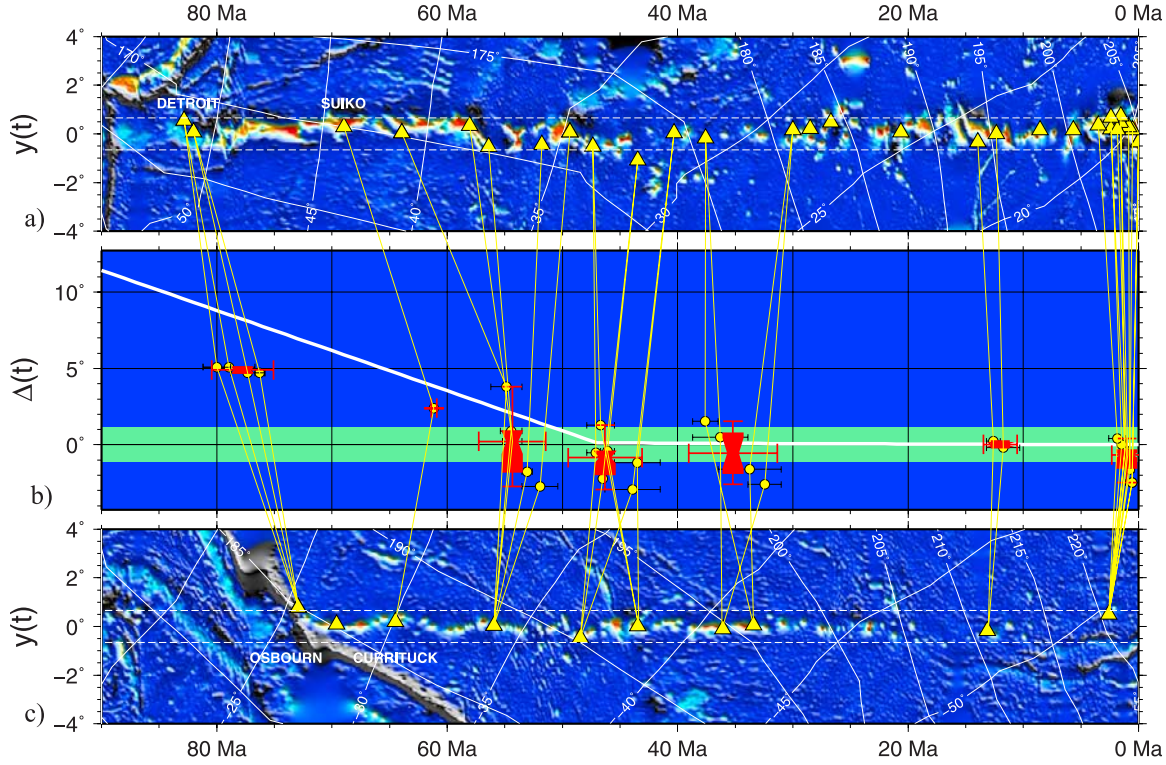

Figure 12. Plate tectonic projection [see *Wessel et al.*, 2006] of seafloor within ±4° of the predicted trail determined for the (a) Hawaii-Emperor and (c) Louisville chains. Original longitude-latitude gridlines are shown in white, and yellow triangles represent dated samples; both Figures 12a and 12c have predicted age along the horizontal axis. Dashed white lines demark areas ±75 km from the center track. (b) Observed ages along horizontal axis. Yellow circles represent intersample distances. Red box-and-whisker symbols (with notch width indicating the uncertainty in the median) indicate $\Delta(t)$, the deviation of the computed interchain distances between similarly aged samples relative to the observed hot spot separation (green band indicate 95% error on expected $\Delta(t)$). Thick white line indicates predicted HI-LV interhot spot distance for a moving hot spot model [*Steinberger and Gaina*, 2007].

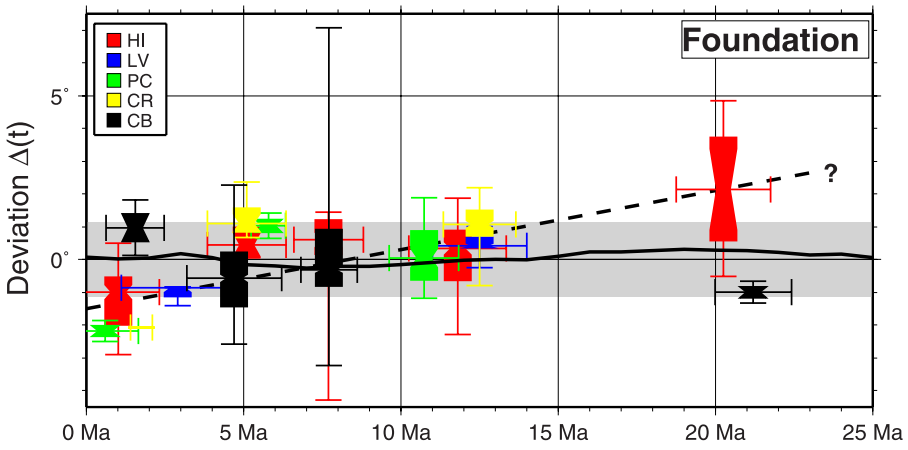

Figure 13. Examination of distances between similarly aged samples from the Foundation chain and five other contemporary chains. All distances have been converted to deviations $\Delta(t)$ from the corresponding inter–hot spot separation and summarized by the notched box-and-whisker diagrams. Gray band is 95% uncertainty on separation. Only the HI-FD separation seems to have a trend with age (dashed line), but it is not significant at the 95% level of confidence. Solid line is a prediction of FD motion relative to HI (B. Steinberger, personal communication, 2006).

deviations of ~2.5° for the Suiko, HI [60.9 Ma], to Currituck, LV [61.4 Ma], separation and ~5° for the Detroit [75.8–81.2 Ma] to Osbourn [76.7–78.8 Ma] separation. This increasing trend is generally reflected in hot spot drift calculations [e.g., *Steinberger and Gaina*, 2007] although they tend to predict a changing separation that often continues through the HEB event [e.g., *Steinberger et al.*, 2004].

[24] However, some care is needed to interpret Figure 12. First, while the larger populations of samples from the post-HEB period allow assessment of how age uncertainties map into Δ(t) uncertainties, the scarcity of samples for the pre-HEB period yields no such information and thus their box-and-whisker diagrams falsely convey a sense of small Δ(t) uncertainties. If the uncertainty in Δ(55 Ma) is any indication of expected variability, then the discrepancy in Δ(61 Ma) at Suiko may not be significant. Second, the orientations of the two trails with respect to the great circles connecting the sample groups change considerably as we move from the post- to pre-HEB intervals. In both cases the uncertainty in ages means we have along-track uncertainty. In the post-HEB case, the effect on the great circle separation is relatively minor, as the trail and great circle is approximately perpendicular. However, for the pre-HEB case, the along-track uncertainties are exactly aligned with the great circle, thus maximizing the effect of age uncertainty. These considerations cast some doubt on the significance of the outlying values in Figure 12. We note that *Andrews et al.* [2006], using completely different methods, also found no significant drift up to 67.7 Ma.

[25] Because the oldest chains in our model have extinct hot spots it is not possible to obtain a reference interhot spot distance for these chains. However, for the remaining chains with active (or very recently active) hot spots we can use the optimal hot spot locations to estimate these separations. In comparing all possible hot spot chain pairs we only found a possible departure from the expected separation involving the Foundation chain (Figure 13). Reducing distances by the expected hot spot separation for each pair, we display all intersample observed distance deviations versus age on a single graph. With most of the data showing insignificant variations, the HI-FD separations appear to have a slight trend (dashed line) which is strongly influenced by the outlying points at ~20 Ma. Since the HI-LV separation was constant up to ~55 Ma (for two chains over 70° apart) we find it more likely that it is the Foundation chain that may deviate from the Hawaii reference trend. Most predictions for Foundation hot spot drift relative to Hawaii show no significant variations (B. Steinberger, personal communication, 2006; solid line), but it is possible that the Foundation trail is not a true hot spot chain, having instead originated as a self-sustaining propagating weakness [e.g., *Hieronymus and Bercovici*, 2000] since its inception around 22 Ma [e.g., *Hekinian et al.*, 1999, 1997; *Wessel and Kroenke*, 2007]. However, the analysis in Figure 13 is clearly not conclusive.

3.3. A Revised Pacific Apparent Polar Wander Path

[26] By reconstructing the North Pole using our APM model we obtain a predicted apparent polar wander path for the Pacific, reflecting how the North Pole would seem to move to an observer on the mobile Pacific. These reconstructions of past spin axis positions can be directly compared with estimates of paleomagnetic poles (also assumed to be past spin axis positions) derived from seamount magnetization, drill cores, and the skewness of marine magnetic anomalies (Figure 14). Here, we use recent compilations of the best average paleomagnetic poles since the Early Cretaceous [*Beaman et al.*, 2007; *Sager*, 2006]. It has long been clear that fixed hot spot APM models yield APWPs which roughly trend south and then hook west for ages >100 Ma [*Cox and Gordon*, 1984; *Larson and Lowrie*, 1975; *Larson and Sager*, 1992]. However, ours is the first APM that is self-consistent and has 95% confidence ellipses for reconstructions back to 145 Ma. Unfortunately, there are only a few Pacific paleomagnetic poles that have been determined for the Early Creatceous, and they show large internal disagreements depending on whether or not anomalous skewness is considered [e.g., *Cande*, 1976; *Dyment*

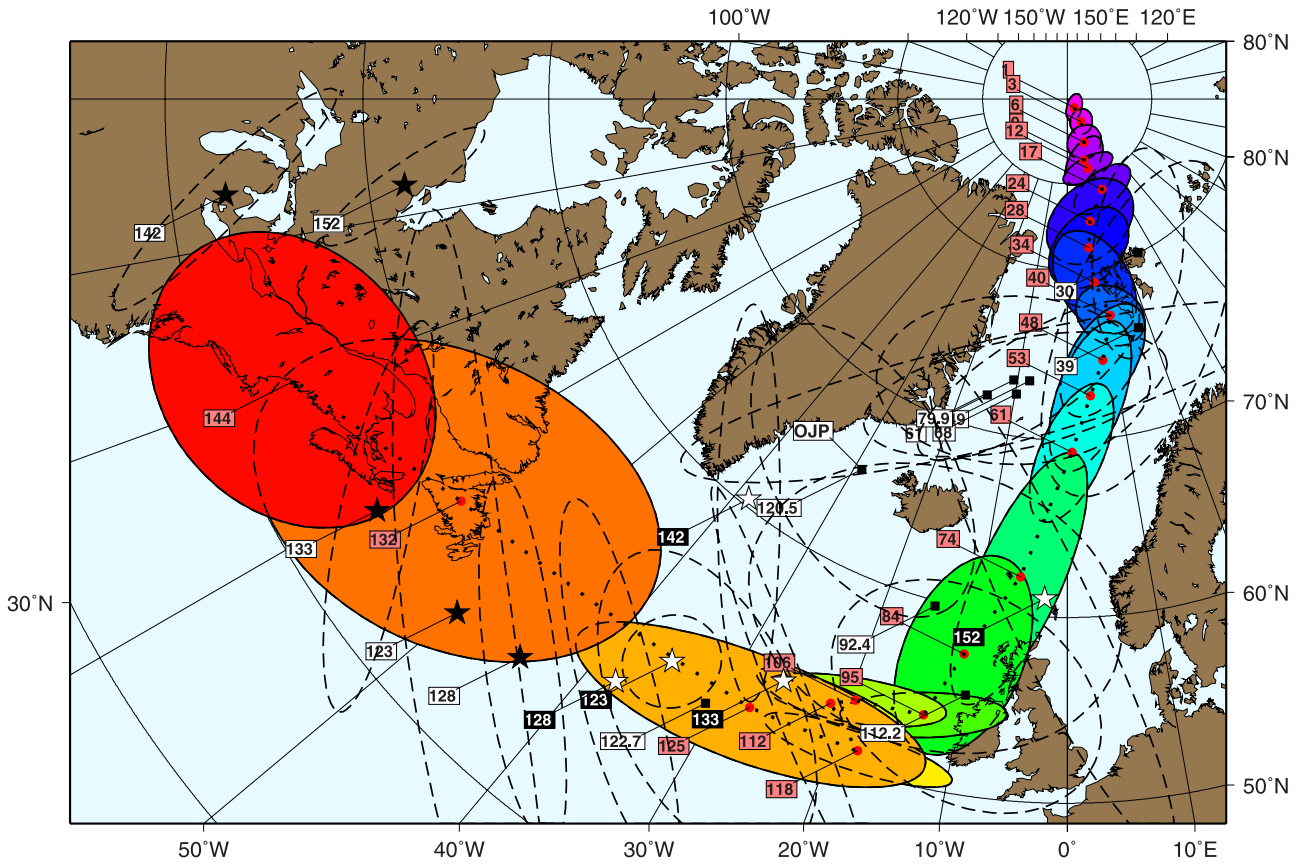

Figure 14. Apparent polar wander paths (APWP) for the Pacific plate. Red circles and corresponding colored error ellipses are APWP predictions from our WK08-A APM model. Black squares are Cretaceous average group paleomagnetic poles from *Sager* [2006] with earlier poles from *Larson and Sager* [1992], here reproduced as stars (black for solutions with anomalous skewness, white without skewness). Anomalous pole for Ontong Java Plateau (OJP; 122 Ma) is also shown.

and Arkani-Hamed, 1995]. We note that *Larson and Sager*'s [1992] poles including anomalous skewness have error ellipses that overlap with our predictions for the same times, but when anomalous skewness is not considered their pole locations fall far from our predictions. It is encouraging that our APM model correlates well with the poles derived with anomalous skewness but, clearly, better defined paleomagnetic poles, including an improved understanding of anomalous skewness, would be required to properly test the validity of our APWP predictions.

3.4. Paleolatitudes and True Polar Wander

[27] Figure 15 shows our predicted paleolatitudes of the Hawaiian hot spot at the times for which paleomagnetic poles are available (blue circles), as well as direct paleolatitude observations (red triangles) from the Emperor seamounts [*Tarduno et al.*, 2003]. For each time t, our predictions are obtained by rotating the paleomagnetically determined spin axis $\mathbf{N}(t)$ to the North Pole, $\mathbf{N}'(t)$, then using the same rotation to rotate our WK08-A-derived spin axis $\mathbf{P}(t)$ to $\mathbf{P}'(t)$. A second rotation is found that moves $\mathbf{P}'(t)$ to the North pole, a rotation which also rotates $\mathbf{N}'(t)$ to $\mathbf{N}''(t)$. In this hot spot reference coordinate system, the difference in distance between the Hawaii hot spot and $\mathbf{N}''(t)$ yields the paleocolatitude at time t. While the linear drift of latitudes proposed by *Tarduno et al.* [2003] is solely derived from the Emperor paleolatitudes, the indirect observations (which depends on our fixed hot spot APM model) confirm this trend to be within the error of the predictions. However, for even older ages (90–144 Ma) the predictions drop back to latitudes indistinguishable (except perhaps for 144 Ma) from that of the Hawaii hot spot. These differences represent motion between the Pacific hot spot reference frame and the paleomagnetic (i.e., spin) axis and could reflect coherent drift of the Pacific hot spots, true polar wander, or a combination of these mechanisms. We are not sure how to interpret the general agreement between inferred and predicted paleolatitudes for the Emperor seamounts or how to explain the return to Hawaii-like latitudes for older ages. However, as plate rotations determined with moving rather than fixed hot spots are quite different, we would have expected a general mismatch between the inferred and predicted paleolatitudes and a degraded fit to the 70–110 Ma sections in our APM model. Thus, we speculate that perhaps the paleolatitudes are, to a large extent, reflecting a true polar wander episode and that hot spot motions for this period have been somewhat overstated. We note that preliminary assessments of TPW based on Africa and Pacific APM models suggest the paleolatitude anomalies can be explained by TPW [e.g., *Gordon and*

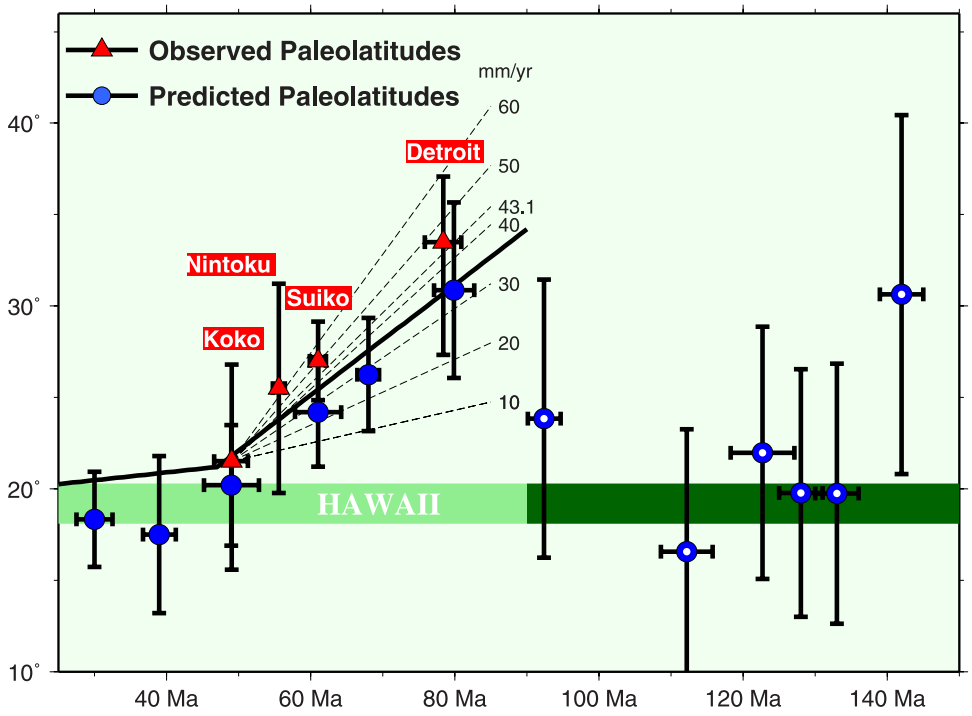

Figure 15. Estimated Hawaii hot spot paleolatitudes (blue circles) for 30, 39, 49, 61, 68, and 79.9 Ma and extrapolated for 92.4, 112.2, 128, 133, and 144 Ma, with approximate error bars. Red triangles and error bars are inferred paleolatitudes for Emperor seamounts [*Tarduno et al.*, 2003]. Black line indicates typical predicted paleolatitudes for a moving hot spot model [*Steinberger and Gaina*, 2007]. Circles with white dots are predictions for ages reflecting the subducted (>90 Ma) portion of the Hawaii-Emperor chain. Dashed lines are inferred hot spot drift rates from *Tarduno et al.* [2003]. Green band reflects present latitude of the Hawaii hot spot.

Horner-Johnson, 2004; *Harada and Wessel*, 2003], yet others argue there was little TPW during the Emperor stage [e.g., *Torsvik et al.*, 2002].

4. Discussion

[28] Our APM models provide a satisfactory fit to both the geometry and chronology of most Pacific chains thought to have been formed at hot spots for the last 145 Ma. Predictions of paleomagnetic latitudes match inferred paleolatitudes for the Emperor seamounts. Thus, the APM models appear to satisfy much of the data available to us. However, several issues are worth discussing further.

[29] First, although the data are sparse, we did observe a ~5° increase in distance between similarly aged samples from the oldest parts of the Emperor and Louisville chains (Figure 12). This discrepancy can only be explained by (1) differential hot spot motion, (2) gross errors in some of the ages, or (3) some seamounts were not formed directly above a hot spot. Explanation 1 is straightforward, in agreement with *Steinberger*'s [2000] predictions, and favored by paleomagneticians [e.g., *Tarduno and Cottrell*, 1997; *Tarduno et al.*, 2003]. Explanation 2 seems unlikely since both segments have recently been redated using the latest analytical techniques [*Koppers et al.*, 2004; *Sharp and Clague*, 2006]. While earlier age estimates were in general agreement with a fixed hot spot prediction, the new dates seem to violate those predictions. Explanation 3 would imply that as the Kula-Pacific spreading center overrode the Hawaiian hot spot (perhaps around ~78 Ma [e.g., *Steinberger and Gaina*, 2007]), the mantle plume continued to channel melt toward the spreading center [e.g., *Small*, 1995], thus producing seamounts further north than its location in the mantle. This possibility was raised by *Tarduno et al.* [2003] but dismissed as they believed its effect was only likely north of Detroit seamount based on their inferred monotonic age progression from Detroit to Koko. However, *Sharp and Clague* [2006] now show a much slower propagation rate between Suiko and Detroit than between Suiko and Koko. This slow age progression is consistent with asthenospheric channeling toward the ridge to the north and furthermore would make inferred paleolatitudes reflect higher latitudes than the actual hot spot location. Of course, explanations 1–3 are not mutually exclusive, and the latter explanation may only explain up to 3–4° of the latitude anomalies [e.g., *Kopp et al.*, 2003]. However, a 3–4° northerly shift would easily explain our observed ~5° increase in intersample separation between Detroit and Osbourn (Figure 12).

[30] Second, while overlapping trails provide a mechanism to extend our APM analysis back in time, they also add a second set of unknowns; the extinct hot spot locations for older chains cannot be verified independently of our APM model. While final hot spot locations (active and extinct) were optimized using hot spotting [e.g., *Wessel and Kroenke*, 1997], many of the extinct hot spots do not benefit from the large HEB APM change in generating a strong

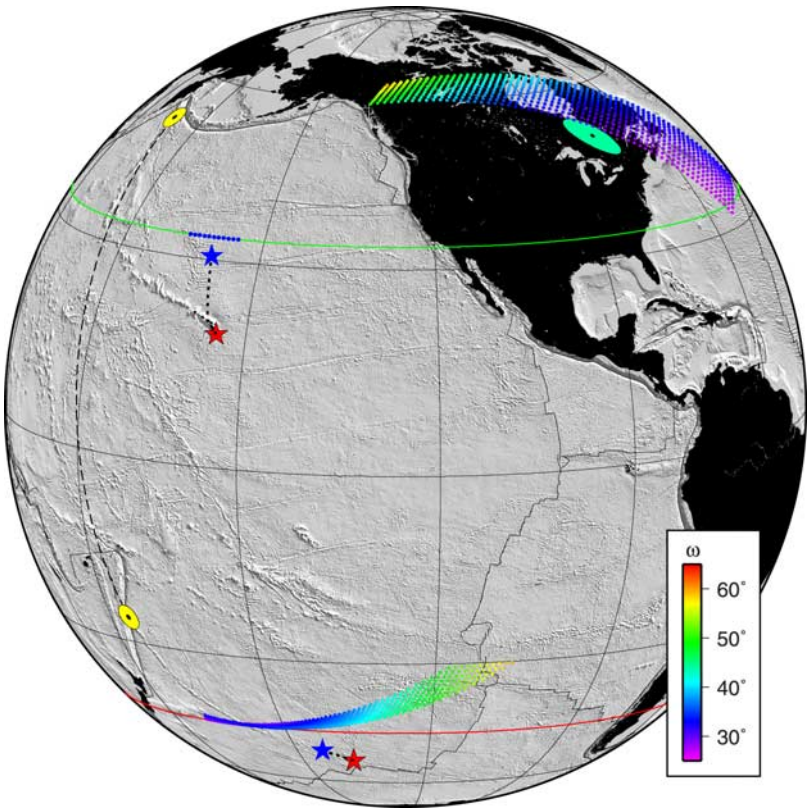

Figure 16. Example of geometric constraints on hot spot motion for Hawaii and Louisville. Yellow ellipses are approximate location uncertainties for the two ~78 Ma old seamounts (Detroit, HI; and Osbourn, LV) separated by $\Delta = 78.2°$ (dashed line). Detroit has a paleolatitude of ~33.5°N (northern green line); hence the Hawaii hot spot at 78 Ma should lie along this latitude. No paleolatitude is available for Osbourn, but given the observed Δ, the Louisville hot spot at 78 Ma cannot be farther south than 44.7°S (red line). Red stars are present hot spot locations (Table 1), with blue stars (and trailing dotted lines) indicating the predictions of *Steinberger and Gaina* [2007]. Blue dots along green line are trial 78 Ma locations for the Hawaii hot spot. For each trial location we can solve for all possible rotation poles and Louisville hot spot locations (rainbow-colored dots) that satisfy the above criteria. For reference, the green ellipse is our 78 Ma fixed hot spot rotation pole derived from WK08-A.

cross-track signature at the optimal hot spot locations. However, the many large APM changes prior to the HEB do yield strong cross-track signatures that we used to optimize the location of extinct hot spots. From a regional geology point of view, the locations of extinct hot spots seem far from ideal. For instance, it would have been preferable to have extinct hot spots located in or near regions that show evidence of past or recent volcanism, but this is generally not the case. Given that much hot spot-related volcanism in the Pacific appears short-lived or has been intermittent [e.g., *Dickinson*, 1998; *Koppers et al.*, 2003; *McNutt et al.*, 1997], this lack of geologic correlation is not considered a fatal shortcoming of the hot spot hypothesis but it certainly does not strengthen it. Because of the short-lived nature of many chains, the Hawaii-Louisville pair takes on a central role in connecting the Tertiary and Cretaceous APM models for the Pacific.

[31] Third, while we believe it is reasonable that age misfits should increase with increasing seamount ages, the larger uncertainties for ages older than ~70 Ma could also mask a significant component of along-trail differential hot spot motion. It is difficult to separate such a signal from the background scatter without a much larger population of seamount ages. The fact that the seamount age database used in this project (see section 2.3) contains a heterogeneous mix of recently dated samples (believed to be of high quality and more accurate) and determinations from 1980 and earlier (considered less reliable) is problematic. The redating of the oldest Louisville samples which yielded corrections of up to 15% [*Koppers et al.*, 2004] illustrates the problem of working with an intrinsically inconsistent data set. On the other hand, differential across-track hot spot motion would be easier to detect as the chain geometries put more stringent constraints on such components of motion.

[32] Fourth, APM modeling with moving hot spots is still dependent on predictions of hot spot motion from geodynamic models. Such modeling is valuable in presenting hot spot motions for reasonable choices of mantle rheology, plate motion history, and initial density conditions inferred from present tomography. However, for older ages the backward convection calculations to model past flow fields start to degrade, as thermal diffusion is inherently a forward process [e.g., *Bunge et al.*, 2003; *Conrad and Gurnis*, 2003; *Steinberger and O'Connell*, 1998]. It is therefore preferable

to constrain APM models with actual observations. Between geometry, chronology, and paleolatitudes we have considerable constraints on what combinations of rigid plate rotations and hot spot motions might be allowed. However, even if there were plentiful paleolatitude determinations along the chains, there might still remain some longitudinal uncertainty. Consider the paleolatitudes for Detroit seamount and its present distance from the coeval Osbourn seamount. These values place limits on where the Louisville hot spot must have been at the time these seamounts where formed (Figure 16); this constraint in turn reduces the domain of possible APM rotations. While only shown for two hot spots here, additional hot spots can add further geometric constraints since coeval seamounts in different trails reflect the distances between the hot spots at the time the seamounts were formed. Further study of these relationships and the addition of more widespread paleolatitude determinations and improved ages would strengthen APM and hot spot drift modeling and provide estimates independent from those of mantle flow calculations. Conversely, careful geometric analysis, such as in Figure 16, might provide further constraints on geodynamic modeling of hot spot motions and improve the ''ranking and selection'' criteria used to cull acceptable hot spot motion candidates [e.g., *O'Neill et al.*, 2005].

[33] **Acknowledgments.** This work was supported by NSF grant OCE-05-26496. Careful reviews by the Associate Editor, Bernard Steinberger, and Anthony Koppers greatly improved the paper. This is SOEST contribution 7444.

References

Andrews, J. A. (1985), True polar wander: An analysis of Cenozoic and Mesozoic paleomagnetic poles, *J. Geophys. Res.*, *90*(B9), 7737–7750.

Andrews, D. L., R. G. Gordon, and B. C. Horner-Johnson (2006), Uncertainties in plate reconstructions relative to the hotspots: Pacific-hotspot rotations and uncertainties for the past 68 million years, *Geophys. J. Int.*, *166*(2), 939–951, doi:10.1111/j.1365-246X.2006.03029.x.

Beaman, M., W. W. Sager, G. D. Acton, L. Lanci, and J. Pares (2007), Improved Late Cretaceous and Early Cenozoic Paleomagnetic apparent polar wander path for the Pacific plate, *Earth Planet. Sci. Lett.*, *262*(1–2), 1–20, doi:10.1016/j.epsl.2007.05.036.

Bonneville, A., et al. (2002), Arago seamount: The missing hotspot found in the Austral Islands, *Geology*, *30*(11), 1023–1026, doi:10.1130/0091-7613(2002)030<1023:ASTMHF>2.0.CO;2.

Bunge, H.-P., C. R. Hagelberg, and B. J. Travis (2003), Mantle circulation models with variational data assimilation: inferring past mantle flow and structure from plate motion histories and seismic tomography, *Geophys. J. Int.*, *152*(2), 280–301, doi:10.1046/j.1365-246X.2003.01823.x.

Cande, S. C. (1976), A paleomagnetic pole from Late Cretaceous marine magnetic anomalies in the Pacific, *Geophys. J. R. Astron. Soc.*, *44*, 547–566.

Cande, S. C., and W. F. Haxby (1991), Eocene propagating rifts in the southwest Pacific and their conjugate features on the Nazca plate, *J. Geophys. Res.*, *96*(B12), 19,609–619,622, doi:10.1029/91JB01991.

Cande, S. C., E. M. Herron, and B. R. Hall (1982), The early Cenozoic tectonic history of the southeast Pacific, *Earth Planet. Sci. Lett.*, *57*, 63–74, doi:10.1016/0012-821X(82)90173-X.

Chang, T. (1987), On the statistical properties of estimated rotations, *J. Geophys. Res.*, *92*(B7), 6319–6329, doi:10.1029/JB092iB07p06319.

Clague, D., and G. B. Dalrymple (1989), The tectonic and geologic setting of the Hawaiian-Emperor volcanic chain, in *The Geology of North America*, vol. N, *The Eastern Pacific Ocean and Hawaii*, edited by E. L. Winterer et al., pp. 188–217, Geol. Soc. of Am., Boulder, Colo.

Clouard, V., and A. Bonneville (2005), Ages of seamounts, islands, and plateaus on the Pacific plate, in *Plates, Plumes, and Paradigms*, edited by G. R. Foulger et al., pp. 71–90, Geol. Soc. of Am., Boulder, Colo.

Conrad, C. P., and M. Gurnis (2003), Seismic tomography, surface uplift, and the breakup of Gondwanaland: Integrating mantle convection backwards in time, *Geochem. Geophys. Geosyst.*, *4*(3), 1031 doi:10.1029/2001GC000299.

Cosca, M. A., R. J. Arculus, J. A. Pearce, and J. G. Mitchell (1998), $^{40}Ar/^{39}Ar$ and K-Ar geochronological age constraints for the inception and early evolution of the Izu-Bonin-Mariana arc system, *Isl. Arc*, *7*, 579–595, doi:10.1111/j.1440-1738.1998.00211.x.

Cox, A., and D. Engebretson (1985), Change in motion of the Pacific plate at 5 Ma BP, *Nature*, *313*, 472–474, doi:10.1038/313472a0.

Cox, A., and R. G. Gordon (1984), Paleolatitudes determined from paleomagnetic data from vertical cores, *Rev. Geophys. Space Phys.*, *22*, 47–72, doi:10.1029/RG022i001p00047.

Cox, R. T. (1999), Hawaiian volcanic propagation and Hawaiian swell asymmetry: evidence of northwestward flow of the deep upper mantle, *Tectonophysics*, *310*, 69–79, doi:10.1016/S0040-1951(99)00151-1.

Dalrymple, G. B., D. A. Clague, and T. L. Vallier (1987), $^{40}Ar/^{39}Ar$ age, petrology, and tectonic significance of some seamounts in the Gulf of Alaska, in *Seamounts, Islands, and Atolls*, edited by B. H. Keating et al., pp. 297–315, AGU, Washington, D. C.

Dana, J. D. (1849), *United States Exploring Expedition, During the Years 1838–1839, 1840, 1841, 1842*, vol. 10, *Geology,* Sherman, C., Philadelphia, Pa.

Dickinson, W. R. (1998), Geomorphology and geodynamics of the Cook-Austral island-seamount chain in the South Pacific Ocean: Implications for hotspots and plumes, *Int. Geol. Rev.*, *40*, 1039–1075.

Dilles, J. H., and P. B. Gans (1995), The chronology of Cenozoic volcanism and deformation in the Yerington area, western Basin and Range and Walker Lane, *Geol. Soc. Am. Bull.*, *107*(4), 474–486, doi:10.1130/0016-7606(1995)107<0474:TCOCVA>2.3.CO;2.

Duncan, R. A., and R. A. Keller (2004), Radiometric ages for basement rocks from the Emperor Seamounts, ODP Leg 197, *Geochem. Geophys. Geosyst.*, *5*, Q08L03, doi:10.1029/2004GC000704.

Duncan, R. A., T. L. Vallier, and D. A. Falvey (1985), Volcanic episodes at 'Eua, Tonga Islands, in *Geology and Offshore Resources of Pacific Island Arcs—Tonga Region*, edited by D. W. Scholl, and T. L. Vallier pp. 281–290, Circum-Pac. Counc. for Energy and Miner. Resour., Houston, Tex.

Dyment, J., and J. Arkani-Hamed (1995), Spreading-rate-dependent magnetization of the oceanic lithosphere inferred from the anomalous skewness of marine magnetic anomalies, *Geophys. J. Int.*, *121*, 789–804, doi:10.1111/j.1365-246X.1995.tb06439.x.

Epp, D. (1984), Possible perturbations to hotspot traces and implications for the origin and structure of the Line Islands, *J. Geophys. Res.*, *89*(B13), 11,273–11,286, doi:10.1029/JB089iB13p11273.

Foulger, G. R., and J. H. Natland (2003), Is ''hotspot'' volcanism a consequence of plate tectonics?, *Science*, *300*, 921–922, doi:10.1126/science.1083376.

Gordon, R. G., and B. C. Horner-Johnson (2004), Latitudinal shift of the Hawaiian hotspot: Motion relative to other hotspots or true polar wander?, *Eos Trans. AGU*, *85*(47), Fall Meet. Suppl., Abstract V51B-0541.

Handschumacher, D. W. (1976), Post-Eocene plate tectonics of the eastern Pacific, in *The Geophysics of the Pacific Ocean Basin and Its Margins*, *Geophys. Monogr. Ser.*, vol. 9, edited by G. H. Sutton et al., pp. 117–202, AGU, Washington, D. C.

Harada, Y., and Y. Hamano (2000), Recent progress on the plate motion relative to hotspots, in *The History and Dynamics of Global Plate Motions*, *Geophys. Monogr. Ser.*, vol. 121, edited by M. A. Richards et al., pp. 327–338, AGU, Washington, D. C.

Harada, Y., and P. Wessel (2003), Motion of hotspots relative to the paleomagnetic axis, *Eos Trans. American Geophysical Union*, *84*(46), Fall Meet. Suppl., Abstract V31F-04.

Hekinian, R., et al. (1997), Intraplate versus ridge volcanism on the Pacific-Antarctic Ridge near 37°S–111°W, *J. Geophys. Res.*, *102*(B6), 12,265–12,286, doi:10.1029/96JB03856.

Hekinian, R., et al. (1999), Ridge-hotspot interaction: the Pacific-Antarctic Ridge and the Foundation seamounts, *Mar. Geol.*, *160*(3–4), 199–223, doi:10.1016/S0025-3227(99)00027-4.

Hey, R. N. (1977), Tectonic evolution of the Cocos-Nazca spreading center, *Geol. Soc. Am. Bull.*, *88*, 1414–1420.

Hieronymus, C. F., and D. Bercovici (2000), Non-hotspot formation of volcanic chains: control of tectonic and flexural stresses on magma transport, *Earth Planet. Sci. Lett.*, *181*, 539–554, doi:10.1016/S0012-821X(00)00227-2.

Ingersoll, R. V., and P. E. Rumelhart (1999), Three-stage evolution of the Los Angeles basin, southern California, *Geology*, *27*(7), 593–596, doi:10.1130/0091-7613(1999)027<0593:TSEOTL>2.3.CO;2.

Kamp, P. J. J. (1991), Late Oligocene Pacific-wide tectonic event, *Terra Nova*, *3*, 65–69, doi:10.1111/j.1365-3121.1991.tb00845.x.

Kopp, H., C. Kopp, J. Phipps Morgan, E. R. Flueh, and W. Weinrebe (2003), Fossil hot spot-ridge interaction in the Musicians Seamount Province: Geophysical investigations of hot spot volcanism at volcanic elongated ridges, *J. Geophys. Res.*, *108*(B3), 2160 doi:10.1029/2002JB002015.

Koppers, A. A., and H. Staudigel (2005), Asynchronous bends in Pacific seamount trails: A case for extensional volcanism?, *Science*, *307*, 904–907, doi:10.1126/science.1107260.

Koppers, A. A. P., J. Phipps Morgan, J. W. Morgan, and H. Staudigel (2001), Testing the fixed hotspot hypothesis using $^{40}Ar/^{39}Ar$ age progres-

sions along seamount trails, *Earth Planet. Sci. Lett.*, *185*, 237–252, doi:10.1016/S0012-821X(00)00387-3.

Koppers, A. A. P., H. Staudigel, M. S. Pringle, and J. R. Wijbrans (2003), Short-lived and discontinuous intraplate volcanism in the South Pacific: Hot spots or extensional volcanism?, *Geochem. Geophys. Geosyst.*, *4*(10), 1089 doi:10.1029/2003GC000533.

Koppers, A. A. P., R. A. Duncan, and B. Steinberger (2004), Implications of a nonlinear $^{40}Ar/^{39}Ar$ age progression along the Louisville seamount trail for models of fixed and moving hot spots, *Geochem. Geophys. Geosyst.*, *5*, Q06L02, doi:10.1029/2003GC000671.

Koppers, A. A. P., H. Staudigel, J. Phipps Morgan, and R. A. Duncan (2007), Nonlinear $^{40}Ar/^{39}Ar$ age systematics along the Gilbert Ridge and Tokelau Seamount Trail and the timing of the Hawaii-Emperor Bend, *Geochem. Geophys. Geosyst.*, *8*, Q06L13, doi:10.1029/2006GC001489.

Larson, R. L., and W. Lowrie (1975), Paleomagnetic evidence for motion of the Pacific plate from Leg 32 basalts and magnetic anomalies, *Initial Rep. Deep Sea Drill. Proj.*, *32*, 571–577.

Larson, R. L., and W. W. Sager (1992), Skewness of magnetic anomalies M0 to M29 in the northwestern Pacific, *Proc. Ocean Drill. Program Sci. Results*, *129*, 471–481.

Lithgow-Bertelloni, C., and M. A. Richards (1998), The dynamics of Cenozoic and Mesozoic plate motions, *Rev. Geophys.*, *36*(1), 27–78, doi:10.1029/97RG02282.

Lonsdale, P. (1988), Geography and history of the Louisville hotspot chain in the southwest Pacific, *J. Geophys. Res.*, *93*(B4), 3078–3104, doi:10.1029/JB093iB04p03078.

Lonsdale, P., and K. D. Klitgord (1978), Structure and tectonic history or the eastern Panama basin, *Geol. Soc. Am. Bull.*, *89*, 981–999, doi:10.1130/0016-7606(1978)89<981:SATHOT>2.0.CO;2.

Mahoney, J. J., R. A. Duncan, M. L. G. Tejada, W. W. Sager, and T. J. Bralower (2005), Jurassic-Cretaceous boundary age and mid-ocean-ridge-type mantle source for Shatsky Rise, *Geology*, *33*(3), 185–188, doi:10.1130/G21378.1.

McNutt, M. K., D. W. Caress, J. Reynolds, K. A. Jordahl, and R. A. Duncan (1997), Failure of plume theory to explain midplate volcanism in the southern Austral Islands, *Nature*, *389*, 479–482, doi:10.1038/39013.

Miller, M. S., B. L. N. Kennett, and V. G. Toy (2006), Spatial and temporal evolution of the subducting Pacific plate structure along the western Pacific margin, *J. Geophys. Res.*, *111*, B02401, doi:10.1029/2005JB003705.

Moore, J. G., B. L. Ingram, K. R. Ludwig, and D. A. Clague (1996), Coral ages and island subsidence, Hilo drill hole, *J. Geophys. Res.*, *101*(B5), 11,599–11,605, doi:10.1029/95JB03215.

Morgan, W. J. (1971), Convection plumes in the lower mantle, *Nature*, *230*, 42–43, doi:10.1038/230042a0.

Morgan, W. J. (1972), Plate motions and deep mantle convection, in *Studies in Earth and Space Sciences*, edited by R. Shagam, *Mem. Geol. Soc. Am.*, *132*, 7–22.

Müller, R. D., W. R. Roest, J. Y. Royer, L. M. Gahagan, and J. G. Sclater (1997), Digital isochrons of the world's ocean floor, *J. Geophys. Res.*, *102*(B2), 3211–3214, doi:10.1029/96JB01781.

Norton, I. O. (1995), Plate motions in the North Pacific: The 43 Ma nonevent, *Tectonics*, *14*(5), 1080–1094, doi:10.1029/95TC01256.

O'Neill, C., D. Müller, and B. Steinberger (2005), On the uncertainties in hot spot reconstructions and the significance of moving hot spot reference frames, *Geochem. Geophys. Geosyst.*, *6*, Q04003, doi:10.1029/2004GC000784.

Patriat, P., and J. Achache (1984), India-Eurasia collision chronology has implications for crustal shortening and driving mechanism of plates, *Nature*, *311*, 615–621, doi:10.1038/311615a0.

Pollitz, F. (1986), Pliocene change in Pacific-plate motion, *Nature*, *320*, 738–741, doi:10.1038/320738a0.

Pringle, M. S., and R. A. Duncan (1995), Radiometric ages of basaltic lavas recovered at sites 865, 866, and 869, *Proc. Ocean Drill. Program Sci. Results*, *142–143*, 277–283.

Pringle, M. S., H. Staudigel, and J. Gee (1991), Jasper seamount: Seven million years of volcanism, *Geology*, *19*(4), 364–368, doi:10.1130/0091-7613(1991)019<0364:JSSMYO>2.3.CO;2.

Rona, P. A., and E. S. Richardson (1978), Early Cenozoic global plate reorganization, *Earth Planet. Sci. Lett.*, *40*, 1–11, doi:10.1016/0012-821X(78)90069-9.

Sager, W. W. (2006), Cretaceous paleomagnetic apparent polar wander path for the Pacific plate calculated from Deep Sea Drilling Project and Ocean Drilling Program basalt cores, *Phys. Earth Planet. Inter.*, *156*(3–4), 329–349, doi:10.1016/j.pepi.2005.09.014.

Sager, W. W., and B. Keating (1984), Paleomagnetism of Line Islands seamounts: Evidence for Late Cretaceous and Early Tertiary volcanism, *J. Geophys. Res.*, *89*(B13), 11,135–11,151, doi:10.1029/JB089iB13p11135.

Sager, W. W., J. Kim, A. Klaus, M. Nakanishi, and L. M. Khankishieva (1999), Bathymetry of Shatsky Rise, northwest Pacific Ocean: Implications for ocean plateau development at a triple junction, *J. Geophys. Res.*, *104*(B4), 7557–7576, doi:10.1029/1998JB900009.

Sandwell, D. T., et al. (1995), Evidence for diffuse extension of the Pacific plate from Pukapuka ridges and cross-grain gravity lineations, *J. Geophys. Res.*, *100*(B8), 15,087–15,099, doi:10.1029/95JB00156.

Sharp, W. D., and D. A. Clague (2006), 50-Ma initiation of Hawaii-Emperor bend records major change in Pacific plate motion, *Science*, *313*, 1281–1284, doi:10.1126/science.1128489.

Small, C. (1995), Observations of ridge-hotspot interactions in the Southern Ocean, *J. Geophys. Res.*, *100*(B9), 17,931–17,946, doi:10.1029/95JB01377.

Steinberger, B. (2000), Plumes in a convecting mantle: models and observations for individual hotspots, *J. Geophys. Res.*, *105*(B5), 11,127–11,152.

Steinberger, B., and C. Gaina (2007), Plate-tectonic reconstructions predict part of the Hawaiian hotspot track to be preserved in the Bering Sea, *Geology*, *35*(5), 407–410, doi:10.1130/G23383A.1.

Steinberger, B., and R. J. O'Connell (1998), Advection of plumes in mantle flow: Implications for hot spot motion, mantle viscosity and plume distributions, *Geophys. J. Int.*, *132*, 412–434, doi:10.1046/j.1365-246x.1998.00447.x.

Steinberger, B., R. Sutherland, and R. J. O'Connell (2004), Prediction of Emperor-Hawaii seamount locations from a revised model of global plate motion and mantle flow, *Nature*, *430*, 167–173, doi:10.1038/nature02660.

Tarduno, J. A., and R. D. Cottrell (1997), Paleomagnetic evidence for motion of the Hawaiian hotspot during formation of the Emperor seamounts, *Earth Planet. Sci. Lett.*, *153*(3–4), 171–180, doi:10.1016/S0012-821X(97)00169-6.

Tarduno, J. A., et al. (2003), The Emperor Seamounts: Southward motion of the Hawaiian hotspot plume in Earth's mantle, *Science*, *301*, 1064–1069, doi:10.1126/science.1086442.

Torsvik, T. H., R. Van der Voo, and T. F. Redfield (2002), Relative hotspot motions versus true polar wander, *Earth Planet. Sci. Lett.*, *202*(2), 185–200, doi:10.1016/S0012-821X(02)00807-5.

Turner, D. L., and R. D. Jarrard (1982), K-Ar dating of the Cook-Austral island chain: A test of the hot-spot hypothesis, *J. Volcanol. Geotherm. Res.*, *12*, 187–220, doi:10.1016/0377-0273(82)90027-0.

Wessel, P. (2001), Global distribution of seamounts inferred from gridded Geosat/ERS-1 altimetry, *J. Geophys. Res.*, *106*(B9), 19,431–19,441, doi:10.1029/2000JB000083.

Wessel, P., and L. W. Kroenke (1997), Relocating Pacific hot spots and refining absolute plate motions using a new geometric technique, *Nature*, *387*, 365–369, doi:10.1038/387365a0.

Wessel, P., and L. W. Kroenke (1998), The geometric relationship between hot spots and seamounts: Implications for Pacific hot spots, *Earth Planet. Sci. Lett.*, *158*, 1–18, doi:10.1016/S0012-821X(98)00043-0.

Wessel, P., and L. W. Kroenke (2000), Ontong Java plateau and late Neogene changes in Pacific plate motion, *J. Geophys. Res.*, *105*(B12), 28,255–28,278, doi:10.1029/2000JB900290.

Wessel, P., and L. W. Kroenke (2007), Reconciling late Neogene Pacific absolute and relative plate motion changes, *Geochem. Geophys. Geosyst.*, *8*, Q08001, doi:10.1029/2007GC001636.

Wessel, P., Y. Harada, and L. W. Kroenke (2006), Towards a self-consistent, high-resolution absolute plate motion model for the Pacific, *Geochem. Geophys. Geosyst.*, *7*, Q03L12, doi:10.1029/2005GC001000.

Whittaker, J. M., et al. (2007), Major Australian-Antarctic Plate reorganization at Hawaiian-Emperor bend time, *Science*, *318*, 83–86, doi:10.1126/science.1143769.

Wilson, J. T. (1963), A possible origin of the Hawaiian islands, *Can. J. Phys.*, *41*, 863–870.

Winterer, E. L., and C. V. Metzler (1984), Origin and subsidence of guyots in Mid-Pacific Mountains, *J. Geophys. Res.*, *89*(B12), 9969–9979, doi:10.1029/JB089iB12p09969.

L. W. Kroenke and P. Wessel, School of Ocean and Earth Science and Technology, University of Hawaii at Manoa, 1680 East-West Road, Honolulu, HI 96822-2219, USA. (pwessel@hawaii.edu)